Implied vol for any local-stochastic vol model

Matthew Lorig [*]   Stefano Pagliarani [†]   Andrea Pascucci [‡]

This version: June 23, 2013

Abstract

We consider an asset whose risk-neutral dynamics are described by a general local-stochastic volatility model. In this setting, we derive a family of asymptotic expansions for the transition density of the underlying as well as for European-style option prices and for implied volatilities. Our expansions are numerically efficient. Approximate transition densities and implied volatilities are explicit; they do not require any special functions nor do they require numerical integration. Approximate option prices require only a Normal CDF (as is the case of the Black-Scholes setting). Additionally, we establish rigorous error bounds for our transition density expansion. To illustrate the accuracy and versatility of our implied volatility expansion, we implement this expansion under five different model dynamics: CEV local volatility, quadratic local volatility, Heston stochastic volatility, 3/2 stochastic volatility, and SABR local-stochastic volatility. Our implied volatility expansion is found to perform favorably compared to other well-known expansions for these models.

Keywords: implied volatility, local-stochastic volatility, CEV, Heston, SABR.

1 Introduction

Neither local volatility (LV) nor stochastic volatility (SV) models are able to fit empirically observed implied volatility levels over the full range of strikes an maturities. This has led to the development of local-stochastic volatility (LSV) models, which combine the features of LV and SV models by describing the instantaneous volatility of an underlying S by a function $f(S_t, Z_t)$ where Z is some auxiliary, possibly multidimensional, stochastic process (see, for instance, Lipton (2002), Alexander and Nogueira (2004), Ewald (2005), Henry-Labordere (2009) and Clark (2010)). Compared to their LV and SV counterparts, LSV models produce implied volatility surfaces that more closely match those observed in the market. However, LSV models rarely allow for exact formulas for option prices. Thus, LSV models present two challenges. First, given an LSV model, can one find accurate closed-form approximations for option prices? Second, given approximate option prices, can one find accurate closed-form approximations for implied volatilities?

---

[*]ORFE Department, Princeton University, Princeton, USA. Work partially supported by NSF grant DMS-0739195.

[†]Dipartimento di Matematica, Università di Padova, Padova, Italy

[‡]Dipartimento di Matematica, Università di Bologna, Bologna, Italy

In the area of pricing, there have been a number or recent developments. An exhaustive review of LSV pricing approximations would be prohibitive. However, we mention the following: Lorig (2012) adds multi-scale stochastic volatility to general scalar diffusions, and thus obtains analytically tractable eigenfunction approximations for options prices. Pagliarani and Pascucci (2013) add general local volatility to the Heston model and obtain a Fourier-like representation for approximate option prices.

Typically, unobservable LSV (or SV or LV) model parameters are obtained by calibrating these models to implied volatilities that are observed on the market. To do this, one must find model-induced implied volatilities over a range of strikes and maturities. Computing model-induced implied volatilities from option prices by inverting the Black-Scholes formula numerically is a computationally intensive task, and therefore, not suitable for the purposes of calibration. For this reason closed-form approximations for model-induced implied volatilities are needed. A number of different approach have been taken for computing approximate implied volatilities in LV, SV and LSV models. We review some of these approaches below.

Concerning LV models, perhaps the earliest and most well-known implied volatility result is due to Hagan and Woodward (1999), who use singular perturbation methods to obtain an implied volatility expansion for general LV models. For certain models (e.g., CEV) they obtain closed-form approximations. More recently, Lorig (2013) uses regular perturbation methods to obtain an implied volatility expansion when a LV model can be written as a regular perturbation around Black-Scholes. Jacquier and Lorig (2013) extend and refine the results of Lorig (2013) to find closed-form approximations of implied volatility for local Lévy-type models with jumps. Gatheral, Hsu, Laurence, Ouyang, and Wang (2012) examines the small-time asymptotics of implied volatility for LV models using heat kernel methods.

There is no shortage of implied volatility results for SV models either. Fouque, Lorig, and Sircar (2012) (see also Fouque, Papanicolaou, Sircar, and Solna (2011)) derive an asymptotic expansion for general multi-scale stochastic volatility models using combined singular and regular perturbation theory. Forde and Jacquier (2011) use the Freidlin-Wentzell theory of large deviations for SDEs to obtain the small-time behavior of implied volatility for general stochastic volatility models with zero correlation. Their work adds mathematical rigor to previous work by Lewis (2007). Forde and Jacquier (2009) use large deviation techniques to obtain the small-time behavior of implied volatility in the Heston model (with correlation). They further refine these results in Forde, Jacquier, and Lee (2012).

Concerning LSV models, perhaps the most well-known implied volatility result is due to Hagan, Kumar, Lesniewski, and W (2002), who use WKB approximation methods to obtain implied volatility asymptotics in a LSV model with a CEV-like factor of local volatility and a GBM-like factor of non-local volatility (i.e., the SABR model). More recently, Henry-Labordère (2005) uses a heat kernel expansion on a Riemann manifold to derive first order asymptotics for implied volatility for any LSV model. As an example, he introduces the λ-SABR model, which is a LSV model with a mean reverting non-local factor of volatility, and obtains closed form asymptotic formulas for implied volatility in this setting. See also Henry-Labordère (2009).

There are also some model-free results concerning the extreme-strike behavior of implied volatility. Most notably, we mention the work of Lee (2004) and Gao and Lee (2011).

In this paper, we consider general LSV models. For these models, we derive a family of closed-form asymptotic expansions for transition densities, option prices and implied volatilities. Our method most

closely follows that of Lorig, Pagliarani, and Pascucci (2013) who derive a family of density and option price expansions for scalar Lévy-type processes. Lorig, Pagliarani, and Pascucci (2013) use a very general technique, the so-called Adjoint Expansion method, first introduced by Pagliarani and Pascucci (2012) and Pagliarani, Pascucci, and Riga (2013) (see also Corielli, Foschi, and Pascucci (2010) for previous related results). The major contributions of this manuscript are as follows:

- Whereas Pagliarani and Pascucci (2012) expand the coefficients of a scalar diffusion as a Taylor series about an arbitrary point, i.e. $f(x) = \sum_n a_n(x - \bar{x})^n$, in order to achieve their approximation result, we expand the diffusion coefficients of a multi-dimensional diffusion in an arbitrary basis, i.e. $f(x, y) = \sum_n \sum_h c_{n,h} B_{n,h}(x, y)$. Thus, we not only extend the results of Pagliarani and Pascucci (2012) from one to multiple dimensions, but we also consider more general expansions.

- We provide an explicit formula for the nth term in our transition density and option-price expansions. The terms in the density expansion appear as Hermite polynomials multiplied by Gaussian kernels and thus, can be computed extremely quickly. In Lorig et al. (2013) the nth term of the transition density is given as a Fourier transform, which is computationally more intensive. In Pagliarani et al. (2013), no general formula for the nth term appears.

- We provide closed-form approximations for implied volatility in a general local-stochastic volatility setting. We show (through a series of numerical experiments) that our implied volatility approximation performs favorably when compared to other well-known implied volatility approximations (e.g., Hagan and Woodward (1999) for CEV, Forde, Jacquier, and Lee (2012) for Heston, and Hagan, Kumar, Lesniewski, and Woodward (2002) for SABR).

- Many of the above-mentioned implied volatility approximations rely on some special structure for the underlying diffusion (e.g., fast- or slow-varying volatility, or some particular Riemannian geometry which allows for closed-form computation of geodesics). When these structures are absent, the associated implied volatility expansions will not work. By contrast, our implied volatility approximation works for any LSV model (actually, by the Adjoint Expansion method, jumps can be added as well). Thus, in addition to being highly accurate, our approach is quite general and includes several models of great interest for the financial industry. For instance, to the best of our knowledge, we give the first approximation formula for implied volatilities in the 3/2 stochastic volatility model. Of late, the 3/2 model has attracted much interest due to its ability match market prices for both European-style options as well as variance and volatility derivatives Baldeaux and Badran (2012).

- We provide a general result showing how to pass in a model-free way from a price expansion to an implied volatility expansion.

The rest of this paper proceeds as follows: In Section 2 we present the general class of local-stochastic volatility models. We also list some technical model assumptions. Next, in Section 3 we derive the option-pricing PDE. In Section 4 we derive a formal asymptotic expansion (in fact, a family of asymptotic expansions) for the function that solves the option-pricing PDE. The main result of this Section is Theorem 9, which shows that every term in our price (density) expansion can be written as a differential operator acting

3

on a Black-Scholes price (Gaussian density). We also establish error bounds for our asymptotic price and density expansions in Section 4. In Section 5 we derive our implied volatility results. We do this in two steps. First, in Section 5.1 we show how one can pass in a model-free way from a price expansion to an implied volatility expansion. Next, in Section 5.2 we show that, when the price expansion is as given in Theorem 9, the implied volatility expansion is explicit. That is, the expansion does not require any integration or special functions. In Section 6 we implement our implied volatility expansion under five different model dynamics: CEV local volatility, quadratic local volatility, Heston stochastic volatility, 3/2 stochastic volatility, and SABR local-stochastic volatility. Section 7 reviews our results and suggests directions for future research. Long proofs are given in the Appendix.

2   General local-stochastic volatility models

For simplicity, we assume a frictionless market, no arbitrage, zero interest rates and no dividends. We take, as given, an equivalent martingale measure $\mathbb{P}$, chosen by the market on a complete filtered probability space $(\Omega, \mathcal{F}, \{\mathcal{F}_t, t \geq 0\}, \mathbb{P})$. The filtration $\{\mathcal{F}_t, t \geq 0\}$ represents the history of the market. All stochastic processes defined below live on this probability space and all expectations are taken with respect to $\mathbb{P}$. We consider a strictly positive asset S whose risk-neutral dynamics are given by

$$\left.\begin{aligned}
S_t &= \exp(X_t), \\
\mathrm{d}X_t &= -\frac{1}{2}\sigma^2(X_t, Y_t)\mathrm{d}t + \sigma(X_t, Y_t)\mathrm{d}W_t, & X_0 &= x \in \mathbb{R}, \\
\mathrm{d}Y_t &= \alpha(X_t, Y_t)\mathrm{d}t + \beta(X_t, Y_t)\mathrm{d}B_t, & Y_0 &= y \in \mathbb{R}, \\
\mathrm{d}\langle W, B\rangle_t &= \rho(X_t, Y_t)\,\mathrm{d}t, & |\rho| &< 1.
\end{aligned}\right\} \tag{1}$$

We assume that SDE (1) has a unique strong solution, that σ and β are strictly positive functions and that σ, β, ρ and α are smooth. Sufficient conditions for the existence of a unique strong solution can be found, for example, in Ikeda and Watanabe (1989). We also assume that the coefficients are such that $\mathbb{E}\, S_t < \infty$ for all $t \in [0, \infty)$. The class of models described by (1) enjoys the following features:

- **Local-stochastic volatility**. The diffusion coefficient of X depends both locally on X and non-locally on an auxiliary driving process Y through the function $\sigma(x, y)$.

- **Martingale property**. The drift $-\frac{1}{2}\sigma^2(X, Y)$ of X is chosen so as to ensure that $S = \mathrm{e}^X$ is a martingale (as it must be to rule out arbitrage).

- **Arbitrary Y dynamics**. Both the drift $\alpha(X, Y)$ and diffusion coefficient $\beta(X, Y)$ of the auxiliary driving process Y are allowed to depend on both X and Y.

- **Arbitrary correlation**. The correlation $\rho(X, Y)$ between the Brownian motions W and B is allowed to depend on both X and Y.

Equation (1) includes virtually all one-factor stochastic volatility models, all local stochastic volatility models, and all one-factor local-stochastic volatility models.

Remark 1 (Multi-factor local-stochastic volatility models and time-dependent coefficients)**.** The results of this paper can be extended in a straightforward fashion to include models with n non-local factors of volatility and time-dependent drift and diffusion coefficients:

$$S_t = \exp(X_t),$$

$$dX_t = -\frac{1}{2}\sigma^2(t, X_t, \mathbf{Y}_t)dt + \sigma(t, X_t, \mathbf{Y}_t)dW_t, \qquad X_0 = x \in \mathbb{R},$$

$$dY_t^{(i)} = \alpha^{(i)}(t, X_t, \mathbf{Y}_t)dt + \sum_{i=1}^{n} \beta^{(i,j)}(t, X_t, \mathbf{Y}_t)dB_t^{(j)}, \qquad \mathbf{Y}_0 = \mathbf{y} \in \mathbb{R}^n,$$

$$d\langle W, B^{(i)}\rangle_t = \rho^{(i)}(t, X_t, \mathbf{Y}_t)\, dt, \qquad |\rho^{(i)}| < 1.$$

Though, for simplicity, we restrict our analysis to the case of time-homogenous coefficients and $n = 1$.

3   Transition density and option pricing PDE

Let V_t be the time t value of a European derivative, expiring at time $T > t$ with payoff $H(X_T, Y_T)$. Using risk-neutral pricing, the value V_t of the derivative at time t is given by the conditional expectation of the option payoff

$$V_t = \mathbb{E}[H(X_T, Y_T)|\mathcal{F}_t] = \mathbb{E}[H(X_T, Y_T)|X_t, Y_t].$$

Note that we have used the Markov property of the process (X, Y) to replace the filtration $\mathcal{F}_t$ by the sigma-algebra generated by (X_t, Y_t). Thus, to value a European-style option we must compute functions of the form

$$v(t, x, y) := \mathbb{E}[H(X_T, Y_T)|X_t = x, Y_t = y] = \int_{\mathbb{R}^2} dw\, dz\, p(t, x, y; T, w, z)H(w, z). \tag{2}$$

Here, $p(t, x, y; T, w, z)$ is the transition density of the process (X, Y). Note that, by setting $H = \delta_{w,z}$ (the Dirac mass at (w, z)) the function $v(t, x, y)$ becomes the transition density $p(t, x, y; T, w, z)$ since

$$\int_{\mathbb{R}^2} dw'dz'\, p(t, x, y; T, w', z')\delta_{w,z}(w', z') = p(t, x, y; T, w, z).$$

If the function v, defined by (2), is $C^{1,2}([0, T), \mathbb{R}^2)$, then v satisfies the Kolmogorov Backward equation

$$(\partial_t + \mathcal{A})v = 0, \qquad\qquad v(T, x, y) = H(x, y),$$

where the operator $\mathcal{A}$ is the infinitesimal generator of the process (X, Y), given explicitly by

$$\mathcal{A} = a(x, y)(\partial_x^2 - \partial_x) + \alpha(x, y)\partial_y + b(x, y)\partial_y^2 + c(x, y)\partial_x\partial_y, \tag{3}$$

and where the functions a, b and c are defined as

$$a(x, y) := \frac{1}{2}\sigma^2(x, y), \qquad b(x, y) := \frac{1}{2}\beta^2(x, y), \qquad c(x, y) := \rho(x, y)\sigma(x, y)\beta(x, y).$$

At this stage, it is convenient to define

$$t(s) := T - s, \qquad\qquad u(t(s), x, y) := v(s, x, y).$$

Then, a simple application of the chain rule shows

$$(-\partial_t + \mathcal{A})u = 0, \qquad\qquad u(0, x, y) = H(x, y). \tag{4}$$

In what follows, it will be convenient to characterize the differential operator $\mathcal{A}$ by its action on *oscillating exponential functions* $\psi_{\lambda,\omega}(x, y) := \frac{1}{2\pi}\mathrm{e}^{\mathrm{i}\lambda x + \mathrm{i}\omega y}$. Indeed, observe that

$$\mathcal{A}\psi_{\lambda,\omega}(x, y) = \phi(x, y, \lambda, \omega)\psi_{\lambda,\omega}(x, y), \qquad\qquad \psi_{\lambda,\omega}(x, y) := \frac{1}{2\pi}\mathrm{e}^{\mathrm{i}\lambda x + \mathrm{i}\omega y}$$

where $\phi(x, y, \lambda, \omega)$, referred to as the *symbol* of $\mathcal{A}$, is given by

$$\phi(x, y, \lambda, \omega) = a(x, y)(-\lambda^2 - \mathrm{i}\lambda) + \alpha(x, y)\mathrm{i}\omega - b(x, y)\omega^2 - c(x, y)\lambda\omega.$$

The symbol of $\mathcal{A}$ appears naturally in connection with the Fourier transform as follows. For any $f \in \mathcal{S}(\mathbb{R}^2)$, the Schwartz space or space of rapidly decreasing functions on $\mathbb{R}^2$, we define

$$\text{Fourier Transform :} \qquad [\mathcal{F} f](\lambda, \omega) = \widehat{f}(\lambda, \omega) := \frac{1}{2\pi}\int_{\mathbb{R}^2} \mathrm{d}x\mathrm{d}y\, \mathrm{e}^{-\mathrm{i}\lambda x - \mathrm{i}\omega y}f(x, y),$$

$$\text{Inverse Transform :} \qquad [\mathcal{F}^{-1} \widehat{f}](x, y) = f(x, y) = \frac{1}{2\pi}\int_{\mathbb{R}^2} \mathrm{d}\lambda\mathrm{d}\omega\, \mathrm{e}^{\mathrm{i}\lambda x + \mathrm{i}\omega y}\widehat{f}(\lambda, \omega).$$

Note that

$$\mathcal{A}f(x, y) = \frac{1}{2\pi}\int_{\mathbb{R}^2} \mathrm{d}\lambda\mathrm{d}\omega\, \phi(x, y, \lambda, \omega)\,\mathrm{e}^{\mathrm{i}\lambda x + \mathrm{i}\omega y}\widehat{f}(\lambda, \omega). \tag{5}$$

4   Density and option price expansions

Our goal is to construct an approximate solution of Cauchy problem (4). Extending the approach of Pagliarani and Pascucci (2012) and Lorig, Pagliarani, and Pascucci (2013) for scalar Markov processes to the present multi-dimensional setting, we assume that the symbol of $\mathcal{A}$ admits an expansion of the form

$$\phi(x, y, \lambda, \omega) = \sum_{n=0}^{\infty}\sum_{h=0}^{n} B_{n-h,h}(x, y)\phi_{n-h,h}(\lambda, \omega), \tag{6}$$

where $(B_{i,j})$ is a sequence of analytic *basis functions* satisfying $B_{0,0} = 1$ and where each $\phi_{i,j}(\lambda, \omega)$ is of the form

$$\phi_{i,j}(\lambda, \omega) = a_{i,j}(-\lambda^2 - \mathrm{i}\lambda) + \alpha_{i,j}\,\mathrm{i}\omega - b_{i,j}\,\omega^2 - c_{i,j}\,\lambda\omega.$$

Observe that each $\phi_{i,j}(\lambda, \omega)$ is the symbol of a differential operator $\mathcal{A}_{i,j}$ where

$$\mathcal{A}_{i,j} := \phi_{i,j}(\mathcal{D}_x, \mathcal{D}_y), \qquad\qquad \mathcal{D}_x := -\mathrm{i}\partial_x, \qquad\qquad \mathcal{D}_y := -\mathrm{i}\partial_y,$$

which is the infinitesimal generator of a constant coefficient diffusion in $\mathbb{R}^2$. Noting that

$$\mathcal{A}_{i,j}\psi_{\lambda,\omega}(x,y) = \phi_{i,j}(\lambda,\omega)\psi_{\lambda,\omega}(x,y),$$

we see that, formally, the generator $\mathcal{A}$ can be written as follows

$$\mathcal{A} = \sum_{n=0}^{\infty} \mathcal{A}_n, \qquad\qquad \mathcal{A}_n = \sum_{h=0}^{n} B_{n-h,h}(x,y)\phi_{n-h,h}(\mathcal{D}_x,\mathcal{D}_y). \qquad (7)$$

Note that the basis functions $(B_{i,j})$ can be seen as symbols of the differential operators $B_{i,j}(-\mathtt{i}\partial_\lambda, -\mathtt{i}\partial_\omega)$ since

$$B_{i,j}(-i\partial_\lambda, -\mathtt{i}\partial_\omega)\psi_{x,y}(\lambda,\omega) = B_{i,j}(x,y)\psi_{x,y}(\lambda,\omega).$$

Remark 2. More generally, one could consider a decomposition of ϕ as follows

$$\phi(x,y,\lambda,\omega) = \sum_{n=0}^{\infty}\sum_{h=0}^{n}\sum_{i+j=1}^{2} B^{i,j}_{n-h,h}(x,y)a^{i,j}_{n-h,h}(\mathtt{i}\lambda)^i(\mathtt{i}\omega)^j.$$

However, because this generalization brings with it a significant notational cost (i.e., it introduces two new indices, which one must keep track of), we restrict our analysis to the case where ϕ is given by (6).

Below, we illustrate a few useful choices for basis functions.

Example 3 (Taylor series). In Pagliarani, Pascucci, and Riga (2013), the authors expand the drift and diffusion coefficients of a scalar diffusion as a power series about an arbitrary point. Extending this idea to the multiple dimensions, we fix a point $(\bar{x}, \bar{y}) \in \mathbb{R}^2$ and we expand

$$\left.\begin{aligned}
\alpha(x,y) &= \sum_{n=0}^{\infty}\sum_{h=0}^{n}\alpha_{n-h,h}(x-\bar{x})^{n-h}(y-\bar{y})^h, \quad \alpha_{n-h,h} := \frac{1}{(n-h)!\,h!}\partial_x^{n-h}\partial_y^h\alpha(\bar{x},\bar{y}), \\
a(x,y) &= \sum_{n=0}^{\infty}\sum_{h=0}^{n}a_{n-h,h}(x-\bar{x})^{n-h}(y-\bar{y})^h, \quad a_{n-h,h} := \frac{1}{(n-h)!\,h!}\partial_x^{n-h}\partial_y^h a(\bar{x},\bar{y}), \\
b(x,y) &= \sum_{n=0}^{\infty}\sum_{h=0}^{n}b_{n-h,h}(x-\bar{x})^{n-h}(y-\bar{y})^h, \quad b_{n-h,h} := \frac{1}{(n-h)!\,h!}\partial_x^{n-h}\partial_y^h b(\bar{x},\bar{y}), \\
c(x,y) &= \sum_{n=0}^{\infty}\sum_{h=0}^{n}c_{n-h,h}(x-\bar{x})^{n-h}(y-\bar{y})^h, \quad c_{n-h,h} := \frac{1}{(n-h)!\,h!}\partial_x^{n-h}\partial_y^h c(\bar{x},\bar{y}).
\end{aligned}\right\} \quad (8)$$

Setting $B_{n-h,h}(x,y) = (x-\bar{x})^{n-h}(y-\bar{y})^h$ we observe that (6) and (7) become, respectively

$$\phi(x,y,\lambda,\omega) = \sum_{n=0}^{\infty}\sum_{h=0}^{n}(x-\bar{x})^{n-h}(y-\bar{y})^h\phi_{n-h,h}(\lambda,\omega),$$

$$\mathcal{A} = \sum_{n=0}^{\infty}\sum_{h=0}^{n}(x-\bar{x})^{n-h}(y-\bar{y})^h\phi_{n-h,h}(\mathcal{D}_x,\mathcal{D}_y).$$

where the coefficients $\alpha_{n-h,h}$, $a_{n-h,h}$, $b_{n-h,h}$ and $c_{n-h,h}$ of $\phi_{n-h,h}$ are given in (8).

Example 4 (Two-Point Taylor Series). Consider a local volatility model $dX_t = -\frac{1}{2}\sigma^2(X_t)dt + \sigma(X_t)dW_t$ with generator $\mathcal{A}$ and symbol ϕ given by

$$\mathcal{A} = a(x)(\partial_x^2 - \partial_x), \qquad \phi(x, \lambda) = a(x)(-\lambda^2 - \mathtt{i}\lambda), \qquad a(x) := \frac{1}{2}\sigma^2(x). \qquad (9)$$

For fixed $\bar{x}_0, \bar{x}_1, \bar{x}_2 \in \mathbb{R}$, the function a can be expanded as a *two-point Taylor series* as follows

$$a(x) = a(\bar{x}_0) + \sum_{n=0}^{\infty} (a_n(\bar{x}_0, \bar{x}_1, \bar{x}_2)(x - \bar{x}_1) + a_n(\bar{x}_0, \bar{x}_2, \bar{x}_1)(x - \bar{x}_2)) (x - \bar{x}_1)^n (x - \bar{x}_2)^n, \qquad (10)$$

where

$$a_0(\bar{x}_0, \bar{x}_1, \bar{x}_2) = \frac{a(\bar{x}_2) - a(\bar{x}_0)}{\bar{x}_2 - \bar{x}_1},$$

$$a_n(\bar{x}_0, \bar{x}_1, \bar{x}_2) = \sum_{h=0}^{n} \frac{(h+n-1)!}{h!n!(n-h)!} \frac{(-1)^h h \partial_{\bar{x}_1}^{n-h}[a(\bar{x}_1) - a(\bar{x}_0)] + (-1)^{n+1} n \partial_{\bar{x}_2}^{n-h}[a(\bar{x}_2) - a(\bar{x}_0)]}{(\bar{x}_1 - \bar{x}_2)^{h+n+1}}.$$

For the derivation of this result we refer the reader to Estes and Lancaster (1972); Lopez and Temme (2002). Note that truncating the two-point Taylor series expansion (10) at $n = m$ results in an expansion for a which is of order $\mathcal{O}(x^{2m+1})$. The advantage of using a two-point Taylor series is that, by considering the first n derivatives of a function a at two points $\bar{x}_1$ and $\bar{x}_2$, one can achieve a more accurate approximation of a over a wider range of values than if one were to approximate a using $2n$ derivatives at a single point (i.e., the usual Taylor series approximation).

Using (9) and (10), we can formally express the symbol ϕ as

$$\phi(x, \lambda) = \sum_{n=0}^{\infty} B_n(x)\phi_n(\lambda),$$

where $B_0(x) = 1$, $\phi_0 = -a(\bar{x}_0)(\lambda^2 + \mathtt{i}\lambda)$ and

$$B_n(x) = (a_{n-1}(\bar{x}_0, \bar{x}_1, \bar{x}_2)(x - \bar{x}_1) + a_{n-1}(\bar{x}_0, \bar{x}_2, \bar{x}_1)(x - \bar{x}_2)) (x - \bar{x}_1)^{n-1}(x - \bar{x}_2)^{n-1}, \qquad n \geq 1,$$

$$\phi_n(\lambda) = -(\lambda^2 + \mathtt{i}\lambda), \qquad\qquad\qquad n \geq 1.$$

Example 5 (Non-local approximation in a weighted L^2-space). Let $(B_{i,j})$ be an orthonormal basis in the weighted space $L^2(\mathbb{R}^2, \mathfrak{m}(x, y)dxdy)$. Then $\phi_{i,j}(\lambda, \omega)$ is given by

$$\phi_{i,j}(\lambda, \omega) = \langle \phi(\cdot, \cdot, \lambda, \omega), B_{i,j}(\cdot, \cdot) \rangle_{\mathfrak{m}}.$$

For instance, one could choose the *Hermite polynomials* $\mathbf{H}_n$ centered at $(\bar{x}, \bar{y})$ as basis functions

$$B_{n,h}(x, y) = \frac{\mathbf{H}_n(x - \bar{x})}{\sqrt{(2n)!!\sqrt{\pi}}} \frac{\mathbf{H}_h(y - \bar{y})}{\sqrt{(2h)!!\sqrt{\pi}}}, \qquad \mathbf{H}_n(x) := (-1)^n \frac{\partial_x^n \exp(-x^2)}{\exp(-x^2)}. \qquad (11)$$

Such basis functions are orthonormal under a Gaussian weighting

$$\langle B_{i,j}, B_{h,l} \rangle_{\mathfrak{m}} := \delta_{i,j}\delta_{h,l}, \qquad \mathfrak{m}(x, y) = \exp\left(-(x - \bar{x})^2 - (y - \bar{y})^2\right).$$

Having discussed some useful basis functions, we now return to Cauchy problem (4). We re-write the operator $\mathcal{A}$ in (7) as

$$\mathcal{A} = \sum_{n=0}^{\infty} \varepsilon^n \mathcal{A}_n, \qquad\qquad \varepsilon = 1, \qquad\qquad (12)$$

where we have introduced ε, which serves merely as an accounting feature. Next, we suppose that the solution u can be written as a sum of the form

$$u = u^{\varepsilon} := \sum_{n=0}^{\infty} \varepsilon^n u_n, \qquad\qquad \varepsilon = 1. \qquad\qquad (13)$$

We insert expansions (12) and (13) into PDE (4) and collect terms of like order in ε. We find

$$\mathcal{O}(1): \qquad (-\partial_t + \mathcal{A}_0)u_0 = 0, \qquad\qquad u_0(0, x, y) = H(x, y), \qquad (14)$$

$$\mathcal{O}(\varepsilon^n): \qquad (-\partial_t + \mathcal{A}_0)u_n = -\sum_{h=1}^{n} \mathcal{A}_h u_{n-h}, \qquad u_n(0, x, y) = 0. \qquad (15)$$

Having served its purpose, we set ε to the side. Our goal is to solve Cauchy problems (14) and (15). Observe that u_0, the solution of (14) is well-known

$$u_0(t, x, y) = \int_{\mathbb{R}^2} \mathrm{d}w \mathrm{d}z \, p_0(0, x, y; t, w, z) H(w, z), \qquad\qquad (16)$$

where p_0 is the *fundamental solution* of PDE (14), which is simply the density $f_{\mu, \Sigma}(x, y)$ of a two-dimensional Gaussian random vector with mean vector μ and covariance matrix Σ given by

$$\mu = \begin{pmatrix} w + a_{0,0}t \\ z - \alpha_{0,0}t \end{pmatrix}, \qquad\qquad \Sigma = \begin{pmatrix} 2a_{0,0}t & c_{0,0}t \\ c_{0,0}t & 2b_{0,0}t \end{pmatrix}.$$

Remark 6. In the case of Examples 3, 4 and 5 the matrix Σ is positive definite for any $t > 0$. For instance, consider the Taylor series expansion (Example 3). Using (8) we have $\det(\Sigma) = t\sigma^2(\bar{x}, \bar{y})\beta^2(\bar{x}, \bar{y})(1 - \rho(\bar{x}, \bar{y})) > 0$ by the assumptions on the coefficients σ, β and ρ.

In order to find an explicit expression for the sequence of higher order terms (u_i) we shall first derive an explicit expression for $\widehat{u}_i$, the Fourier transform u_i. We will then use the Fourier representation $\widehat{u}_i$ to show that each u_i can be expressed as a differential operator acting on u_0.

Proposition 7. *Suppose* $H \in L^1(\mathbb{R}^2, \mathrm{d}x\mathrm{d}y)$ *and let* $\widehat{H}$ *denote its Fourier transform. Suppose further that* u_n *and* $\widehat{u}_n$ *exist. Then* $\widehat{u}_0$ *is given by*

$$\widehat{u}_0(t, \lambda, \omega) = \mathrm{e}^{t\phi_{0,0}(\lambda, \omega)} \widehat{H}(\lambda, \omega), \qquad\qquad (17)$$

and $\widehat{u}_n$ $(n \geq 1)$ *is given by*

$$\widehat{u}_n(t, \lambda, \omega) = \sum_{h=1}^{n} \sum_{l=0}^{h} \int_0^t \mathrm{d}s \, \mathrm{e}^{(t-s)\phi_{0,0}(\lambda, \omega)} B_{h-l,l}(\mathrm{i}\partial_\lambda, \mathrm{i}\partial_\omega)\phi_{h-l,l}(\lambda, \omega)\widehat{u}_{n-h}(s, \lambda, \omega), \qquad n \geq 1. \quad (18)$$

Note that the operator $B_{h-l,l}(\mathrm{i}\partial_\lambda, \mathrm{i}\partial_\omega)$ *acts on* <u>*everything*</u> *to the right of it.*

Proof. See Appendix A. □

Remark 8. Proposition 7 is the two-dimensional extension of Corollary 10 from Lorig, Pagliarani, and Pascucci (2013). In that paper, the authors focus on scalar Lévy-type processes. In fact, although we have only considered two-dimensional diffusions in this paper, Proposition 7 remains valid if $\phi(x, y, \lambda, \omega)$ is the symbol of the generator of a two-dimensional Lévy-type process. In the Lévy-type case, due to the complications that arise from jumps, u_n must be expressed as an inverse Fourier transform of $\widehat{u}_n$; it is not possible to find u_n directly. However, because we limit the analysis in this paper to models without jumps, as the following Theorem shows, we are able to find an explicit expression for u_n as a differential operator acting on u_0.

Theorem 9. *For every $n \geq 1$, define*

$$\mathcal{L}_n(t, x, y, \lambda, \omega) = \sum_{h=1}^{n} \int_0^t \mathrm{d}t_1 \cdots \int_0^{t_{k-1}} \mathrm{d}t_h \sum_{\pi \in \Pi_h(n)} \Phi_{\pi(h)}(t_h, t) \cdots \Phi_{\pi(1)}(t_1, t), \qquad (19)$$

where $\Pi_h(n)$ is the set of permutations π such that

$$\Pi_h(n) = \{\pi : \mathbb{N} \to \mathbb{Z}^+ : \sum_{l=1}^{h} \pi(l) = n\},$$

and $\Phi_h(s, t)$ is an abbreviation for the operator

$$\Phi_h(s, t) = \Phi_h(s, t, x, y, \lambda, \omega, -\mathrm{i}\partial_\lambda, -\mathrm{i}\partial_\omega)$$

$$:= \sum_{l=0}^{h} \phi_{h-l,l}(\lambda, \omega) \frac{B_{h-l,l}(-\mathrm{i}\partial_\lambda, -\mathrm{i}\partial_\omega) \mathrm{e}^{\mathrm{i}\lambda x + \mathrm{i}\omega y + (t-s)\phi_{0,0}(\lambda, \omega)}}{\mathrm{e}^{\mathrm{i}\lambda x + \mathrm{i}\omega y + (t-s)\phi_{0,0}(\lambda, \omega)}}, \qquad k \geq 1. \qquad (20)$$

Then $u_n(t, x, y)$, the solution of (15), is given by

$$u_n(t, x, y) = \mathcal{L}_n(t, x, y, \mathcal{D}_x, \mathcal{D}_y) u_0(t, x, y), \qquad n \geq 1, \qquad (21)$$

where u_0 is the solution of Cauchy problem (14). Note that the operators $(\Phi_h)_{h \geq 1}$ act on _everything_ *to the right of them. If nothing appears to the right of the operators $(\Phi_h)_{h \geq 1}$, then they are assumed to act on the constant function: $f = 1$.*

Proof. See Appendix B. □

Remark 10. Note that p_n, the n-th order term in the transition density expansion $p = \sum_{n=0}^{\infty} p_n$, is expressed as a differential operator acting on p_0, which is simply a two-dimensional Gaussian density. Thus, from (11), we see that p_n can be written as a sum of Hermite polynomials multiplied by a Gaussian density.

We now state an asymptotic convergence theorem which extends the results in Pagliarani, Pascucci, and Riga (2013). Define our n-th order approximation for the prices as

$$v^{(n)}(t, x, y) := \sum_{h=0}^{n} u_h(T - t, x, y),$$

10

where the sequence of (u_h) is as given in Theorem 9. The n-th order approximation of the transition density $p^{(n)}(t, x, y; T, z, w)$ is defined as the special case where $H = \delta_{w,z}$.

The following theorem provides an asymptotic pointwise estimate as $t \to T^-$ for the error encountered by replacing the exact transition density p with the n-th order approximation $p^{(n)}$, when expanding the operator $\mathcal{A}$ through the Taylor basis functions described in Example 3.

Theorem 11. *Assume that the functions $a = a(x, y)$, $\alpha = \alpha(x, y)$, $b = b(x, y)$ and $c = c(x, y)$ are differentiable up to order n with bounded and Lipschitz continuous derivatives. Assume that the covariance matrix is bounded and uniformly positive definite. That is,*

$$M^{-1}|\xi|^2 < \begin{pmatrix} \xi_1 & \xi_2 \end{pmatrix} \begin{pmatrix} 2a(x,y) & c(x,y) \\ c(x,y) & 2b(x,y) \end{pmatrix} \begin{pmatrix} \xi_1 \\ \xi_2 \end{pmatrix} < M|\xi|^2, \quad (x,y) \in \mathbb{R}^2, \quad \xi = (\xi_1, \xi_2) \in \mathbb{R}^2 \setminus \{(0,0)\},$$

where M is a positive constant. If $(\bar{x}, \bar{y}) = (x, y)$ or $(\bar{x}, \bar{y}) = (z, w)$ in (8), then we have

$$\left| p(t, x, y; T, z, w) - p^{(n)}(t, x, y; T, z, w) \right| \le g_n(T - t) \Gamma^M(t, x, y; T, z, w),$$

for any $x, y, z, w \in \mathbb{R}$ and $t \in [0, T)$, where Γ^M denotes the Gaussian fundamental solution of the heat operator $M(\partial_{xx} + \partial_{yy}) + \partial_t$ and $g_n(s) = \mathcal{O}\left(s^{\frac{n+1}{2}}\right)$ as $s \to 0^+$.

We omit the proof of Theorem 11, which is based on the *parametrix method* (see, for instance, Pascucci (2011)) and is analogous to the estimates obtained in Pagliarani, Pascucci, and Riga (2013), Theorem 2.3, for the one-dimensional case. We obtain the same order of convergence for short maturities in the two-dimensional case as was previously obtained in the one-dimensional case. As a direct corollary, we also have the following asymptotic estimate for option prices.

Corollary 12. *Under the assumptions of Theorem 11, for any $n \in \mathbb{N}$ we have*

$$\left| v(t, x, y) - v^{(n)}(t, x, y) \right| \le g_n(T - t) \int_{\mathbb{R}^2} \mathrm{d}w \mathrm{d}z \, H(w, z) \, \Gamma^M(t, x, y; T, w, z)$$

for $x, y \in \mathbb{R}$ and $t \in [0, T)$.

5   Implied volatility expansions

European call and put prices are commonly quoted in units of implied volatility rather than in units of currency. In fact, in the financial industry, model parameters for the risk-neutral dynamics of a security are routinely obtained by calibrating to the market's implied volatility surface. Because calibration requires computing implied volatilities across a range of strikes and maturities and over a large set of model parameters, it is extremely useful to have a method of computing implied volatilities quickly.

We shall break this Section into two parts. First, in Section 5.1, we show how to pass in a general and model-independent way from an expansion of option prices to an expansion of implied volatilities. Then, in Section 5.2, we show that when call option prices can be computed as a series whose terms are as given in Theorem 9, the terms in the corresponding implied volatility expansion can be computed explicitly (i.e., without special functions or integrals). As such, *approximate implied volatilities can be computed even faster than approximate option prices*, which require the special function $\mathcal{N}$, the standard normal CDF.

5.1 Implied volatility expansions from price expansions – the general case

To begin our analysis, we assume that one has a model for the log of the underlying $X = \log S$. We fix a time to maturity $t > 0$, an initial value $X_0 = x$ and a call option payoff $H(X_t) = (e^{X_t} - e^k)^+$. Our goal is to find the implied volatility for *this particular call option*. To ease notation, we will suppress much of the dependence on (t, x, k). However, the reader should keep in mind that the implied volatility of the option under consideration *does* depend on (t, x, k), even if this is not explicitly indicated. Below, we provide definitions of the *Black-Scholes price* and *implied volatility*, which will be fundamental throughout this Section.

Definition 13. For a fixed (t, x, k), the *Black-Scholes price* $u^{\mathrm{BS}} : \mathbb{R}^+ \to \mathbb{R}^+$ is given by

$$u^{\mathrm{BS}}(\sigma) := e^x \mathcal{N}(d_+(\sigma)) - e^k \mathcal{N}(d_-(\sigma)), \qquad d_\pm(\sigma) := \frac{1}{\sigma\sqrt{t}}\left(x - k \pm \frac{\sigma^2 t}{2}\right), \tag{22}$$

Where $\mathcal{N}$ is the CDF of a standard normal random variable.

Definition 14. For fixed (t, x, k), the *implied volatility* corresponding to a call price $u \in ((e^x - e^k)^+, e^x)$ is defined as the unique strictly positive real solution σ of the equation

$$u^{\mathrm{BS}}(\sigma) = u. \tag{23}$$

Notice that $[u^{\mathrm{BS}}]^{-1}$ is an analytic function on its domain $((e^x - e^k)^+, e^x)$. For any $u \in ((e^x - e^k)^+, e^x)$, we denote by ρ_u the radius of convergence of the Taylor series of $[u^{\mathrm{BS}}]^{-1}$ about u.

The main result of the Section is the following Theorem:

Theorem 15. *Assume that the call price u admits an expansion of the form*

$$u = u^{\mathrm{BS}}(\sigma_0) + \sum_{n=1}^{\infty} u_n, \tag{24}$$

for some positive σ_0 and some sequence $(u_n)_{n \geq 1}$ where $u_n \in \mathbb{R}$ for all n. If

$$|u - u^{\mathrm{BS}}(\sigma_0)| < \rho_{u^{\mathrm{BS}}(\sigma_0)}, \tag{25}$$

then the implied volatility $\sigma := [u^{\mathrm{BS}}]^{-1}(u)$ is given by

$$\sigma = \sigma_0 + \sum_{n=1}^{\infty} \sigma_n, \tag{26}$$

where the sequence $(\sigma_n)_{n \geq 1}$ is defined recursively by

$$\sigma_n = U_n(\sigma_0) - \frac{1}{n!}\sum_{h=2}^{n} A_h(\sigma_0)\mathbf{B}_{n,h}\big(\sigma_1, 2!\sigma_2, 3!\sigma_1, \ldots, (n-h+1)!\sigma_{n-h+1}\big). \tag{27}$$

In (27), $\mathbf{B}_{n,h}$ denotes the (n, h)-th partial Bell polynomial[1] and

$$U_n(\sigma_0) := \frac{u_n}{\partial_\sigma u^{\mathrm{BS}}(\sigma_0)}, \qquad\qquad n \geq 1, \tag{28}$$

$$A_n(\sigma_0) := \frac{\partial_\sigma^n u^{\mathrm{BS}}(\sigma_0)}{\partial_\sigma u^{\mathrm{BS}}(\sigma_0)}, \qquad\qquad n \geq 2. \tag{29}$$

---

[1]Partial Bell polynomials are already implemented in Mathematica as $\mathrm{BellY}[n, h, \{x_1, \ldots, x_{n-h+1}\}]$.

Proof. We define $u(\varepsilon)$ an analytic function of ε by

$$u(\varepsilon) := u^{\mathrm{BS}}(\sigma_0) + \sum_{n=1}^{\infty} \varepsilon^n u_n, \qquad\qquad \varepsilon \in [0, 1]. \tag{30}$$

Note that $\sigma(\varepsilon) := [u^{\mathrm{BS}}]^{-1}(u(\varepsilon))$ is the composition of two analytic functions; it is therefore an analytic function of ε and admits an expansion about $\varepsilon = 0$ of the form

$$\sigma(\varepsilon) = \sigma_0 + \sum_{n=1}^{\infty} \varepsilon^n \sigma_n, \qquad\qquad \sigma_n = \frac{1}{n!} \partial_\varepsilon^n \sigma(\varepsilon)|_{\varepsilon=0}, \tag{31}$$

which by (25) is convergent for any $\varepsilon \in [0, 1]$. By (30) we also have

$$u_n = \frac{1}{n!} \partial_\varepsilon^n u^{\mathrm{BS}}(\sigma(\varepsilon))|_{\varepsilon=0}. \tag{32}$$

We compute the n-th derivative of the composition of the two functions in (32) by applying the Bell polynomial version of the Faa di Bruno's formula, which can be found in Riordan (1946) and Johnson (2002). We have

$$u_n = \frac{1}{n!} \sum_{h=1}^{n} \partial_\sigma^h u^{\mathrm{BS}}(\sigma_0) \mathbf{B}_{n,h} \left(\partial_\varepsilon \sigma(\varepsilon), \partial_\varepsilon^2 \sigma(\varepsilon), \ldots, \partial_\varepsilon^{n-h+1} \sigma(\varepsilon) \right) |_{\varepsilon=0}. \tag{33}$$

Theorem 15 follows by inserting (31) into (33) and solving for σ_n. $\qquad\square$

In the following Proposition, we will show that the coefficients A_n in (29) can be computed explicitly using an iterative algorithm. In particular, each $A_n(\sigma)$ is a rational function of σ and no special functions appear in its expression.

Proposition 16. *Define the differential operator*

$$\mathcal{J} := t(\partial_x^2 - \partial_x). \tag{34}$$

Then

$$A_n(\sigma) = \frac{P_n(\mathcal{J}) u^{\mathrm{BS}}(\sigma)}{\partial_\sigma u^{\mathrm{BS}}(\sigma)}, \tag{35}$$

where P_n is a polynomial function of order n defined recursively by

$$P_0(\mathcal{J}) = 1,$$
$$P_1(\mathcal{J}) = \sigma\mathcal{J},$$
$$P_n(\mathcal{J}) = \sigma\mathcal{J}P_{n-1}(\mathcal{J}) + (n-1)\mathcal{J}P_{n-2}(\mathcal{J}), \qquad\qquad n \geq 2.$$

Moreover, the coefficients $A_n(\sigma_0)$ can be expressed explicitly in terms of Hermite[2] polynomials.

---

[2]Our thanks to Peter Carr for pointing out the connection to Hermite polynomials.

Proof. First, we recall the classical relation between the Delta, Gamma and Vega for European options in the Black-Scholes setting

$$\partial_\sigma u^{\mathrm{BS}}(\sigma) = \sigma \mathfrak{J} u^{\mathrm{BS}}(\sigma). \tag{36}$$

Next, using the product rule for derivatives we compute

$$\partial_\sigma^{n+1} u^{\mathrm{BS}} = \partial_\sigma^n \left(\partial_\sigma u^{\mathrm{BS}}\right) = \partial_\sigma^n \left(\sigma \mathfrak{J} u^{\mathrm{BS}}\right) = \sum_{h=0}^{n} \binom{n}{h} \left(\partial_\sigma^h \sigma\right) \left(\mathfrak{J}\partial_\sigma^{n-h} u^{\mathrm{BS}}\right) = \left(\sigma \mathfrak{J}\partial_\sigma^n + n\partial_\sigma^{n-1}\mathfrak{J}\right) u^{\mathrm{BS}}. \tag{37}$$

Equation (35) follows from (29) and (37). Now, to show that each of the $A_n(\sigma)$ can be expressed as a sum of Hermite polynomials, we observe that

$$\frac{\partial_x^n \exp\left(-\left(\frac{x-a}{b}\right)^2\right)}{\exp\left(-\left(\frac{x-a}{b}\right)^2\right)} = \frac{(-1)^n}{b^n} \mathbf{H}_n\left(\frac{x-a}{b}\right), \qquad a \in \mathbb{R}, b > 0, \tag{38}$$

where $\mathbf{H}_n$ is the n-th Hermite polynomial, defined in (11). Moreover using the Black-Scholes formula for call options (22) a direct computation shows

$$\mathfrak{J} u^{\mathrm{BS}}(\sigma) = \frac{e^k \sqrt{t}}{\sigma\sqrt{2\pi}} \exp\left(-\left(\frac{x-k-\sigma^2 t/2}{\sigma\sqrt{2t}}\right)^2\right). \tag{39}$$

Thus, using (36) and (39) we obtain

$$\frac{\mathfrak{J}^{n+1} u^{\mathrm{BS}}(\sigma)}{\partial_\sigma u^{\mathrm{BS}}(\sigma)} = \frac{\mathfrak{J}^n \mathfrak{J} u^{\mathrm{BS}}(\sigma)}{\sigma \mathfrak{J} u^{\mathrm{BS}}(\sigma)} = \frac{\mathfrak{J}^n \exp\left(-\left(\frac{x-k-\sigma^2 t/2}{\sigma\sqrt{2t}}\right)^2\right)}{\sigma \exp\left(-\left(\frac{x-k-\sigma^2 t/2}{\sigma\sqrt{2t}}\right)^2\right)} = \frac{t^n}{\sigma} \sum_{h=0}^{n} \binom{n}{h}(-1)^h \frac{\partial_x^{2n-h} \exp\left(-\left(\frac{x-k-\sigma^2 t/2}{\sigma\sqrt{2t}}\right)^2\right)}{\exp\left(-\left(\frac{x-k-\sigma^2 t/2}{\sigma\sqrt{2t}}\right)^2\right)},$$

where, in the last equality, we have used the binomial expansion of $(\partial_{xx} - \partial_x)^n$. Finally, using (38) with $a = k + \frac{\sigma^2 t}{2}$ and $b = \sigma\sqrt{2t}$, we obtain

$$\frac{\mathfrak{J}^n u^{\mathrm{BS}}(\sigma)}{\partial_\sigma u^{\mathrm{BS}}(\sigma)} = \sum_{h=0}^{n-1} \binom{n-1}{h} \frac{t^{\frac{h}{2}}}{\sigma \left(\sigma\sqrt{2}\right)^{2(n-1)-h}} \mathbf{H}_{2(n-1)-h}\left(\frac{x-k-\sigma^2 t/2}{\sigma\sqrt{2t}}\right), \qquad n \geq 1, \tag{40}$$

Combining (35) with (40), we conclude that $A_n(\sigma)$ can be expressed as a sum of Hermite polynomials. In particular, computing $A_n(\sigma)$ does not involve any special functions or integration. $\qquad\square$

Below, using (27) and Proposition 16, we provide explicit expressions for σ_n for $n \leq 3$. For simplicity, we remove the argument σ_0 from $U_n(\sigma_0)$. We have

$$\sigma_1 = U_1,$$

$$\sigma_2 = U_2 - \frac{1}{2}\left(\frac{(k-x)^2}{t\sigma_0^3} - \frac{t\sigma_0}{4}\right) U_1^2,$$

$$\sigma_3 = U_3 + \frac{1}{48}\left(2tU_1^3 + t^2\sigma_0^2 U_1^3 + 12t\sigma_0 U_1 U_2\right)$$

$$+ \frac{1}{6t\sigma_0^4}\left(3U_1^3 - t\sigma_0^2 U_1^3 - 6\sigma_0 U_1 U_2\right)(k-x)^2 + \frac{1}{3t^2\sigma_0^6} U_1^3 (k-x)^4,$$

where the (U_n) are as given in (28).

14

5.2 Implied volatility when option prices are given by Theorem 9.

We now consider the specific case where the sequence of (u_n) is as given in Theorem 9. We will show that, in this particular setting, the expansion (26) is convergent and approximate implied volatilities can be computed without any numerical integration or special functions. We begin with the following observation:

Remark 17. From (16), one can easily show that $u_0 = u^{\mathrm{BS}}(\sqrt{2a_{0,0}})$. Then, our expansion for the price of a European call option (13) in the general local-stochastic volatility setting (1) becomes

$$u = u^{\mathrm{BS}}(\sigma_0) + \sum_{n=1}^{\infty} u_n, \qquad\qquad \sigma_0 = \sqrt{2a_{0,0}}. \qquad (41)$$

From (41), it is clear that our option price expansion is of the form (24). Therefore, we can use Theorem 15 to find approximate implied volatilities.

Note that, in general, computing approximate implied volatilities using Theorem 15 requires numerical integration, as U_n appearing on the right-hand side of (27) contains u_n, which usually must be computed as a numerical integral. However, as the following Proposition shows, when the sequence of (u_n) are as given in Theorem 9, the sequence of (U_n) appearing in (27) can be computed explicitly, with no numerical integration and no special functions.

Proposition 18. *Let the sequence of (u_n) be as given in Theorem 9. Then U_n, defined in (28), are given by*

$$U_n(\sigma_0) = \sum_{h=0}^{N^{(n)}} D_h^{(n)} \mathbf{H}_h \left(\frac{x - k - \sigma_0^2 t/2}{\sigma\sqrt{2t}} \right).$$

where $\sigma_0 = \sqrt{2a_{0,0}}$, the sequence of coefficients $(D_h^{(n)})$ are (t,x,y)-dependent constants, and each $N^{(n)}$ $(n \in \mathbb{N})$ is a finite positive integer.

Proof. From Theorem 9, one can deduce that every u_n is of the form

$$u_n = \sum_{h=0}^{N^{(n)}} C_h^{(n)} \partial_x^h \left(\partial_x^2 - \partial_x \right) u^{\mathrm{BS}}(\sigma_0), \qquad\qquad \sigma_0 = \sqrt{2a_{0,0}}, \qquad (42)$$

where the sequence of $(C_h^{(n)})$ are (t,x,y)-dependent constants and $N^{(n)}$ is a finite positive integer for every n. Both the sequence of coefficients $(C_h^{(n)})$ and the limit of the sum $N^{(n)}$ depend on the choice of basis functions $(B_{i,j}(x,y))$ and can be computed explicitly using (21). However (and we shall emphasize the following) *independent* of the choice of basis function, the general form (42) always holds; this is due to the fact that $B_{0,0}(x,y) = 1$. Now, using (42) we compute

$$U_n(\sigma_0) = \sum_{h=0}^{N^{(n)}} C_h^{(n)} \frac{\partial_x^h \left(\partial_x^2 - \partial_x \right) u^{\mathrm{BS}}(\sigma_0)}{\partial_\sigma u^{\mathrm{BS}}(\sigma_0)} \qquad\qquad \text{(by (28))}$$

$$= \sum_{h=0}^{N^{(n)}} C_h^{(n)} \frac{\partial_x^h \eth u^{\mathrm{BS}}(\sigma_0)}{t\sigma_0 \eth u^{\mathrm{BS}}(\sigma_0)} \qquad\qquad \text{(by (34))}$$

$$= \sum_{h=0}^{N^{(n)}} C_h^{(n)} \frac{\partial_x^h \exp\left(-\left(\frac{x-k-\sigma_0^2 t/2}{\sigma\sqrt{2t}}\right)^2\right)}{t\sigma_0 \exp\left(-\left(\frac{x-k-\sigma_0^2 t/2}{\sigma_0\sqrt{2t}}\right)^2\right)} \qquad\text{(by (39))}$$

$$= \sum_{h=0}^{N^{(n)}} D_h^{(n)} \mathbf{H}_h\left(\frac{x-k-\frac{\sigma_0^2 t}{2}}{\sigma_0\sqrt{2t}}\right), \qquad\text{(by (38))}$$

where we have absorbed some powers of t and σ_0 into $D_h^{(n)}$. $\qquad\square$

To review, when the sequence of (u_n) is as given in Theorem 9, then using Theorem 15 and Propositions 16 and 18, approximate implied volatilities can be computed as a sum of Hermite polynomials in log-*moneyness:* $(k-x)$. We emphasize: *No numerical integration or special functions are required.* Approximate implied volatilities can therefore be computed even more quickly than approximate option prices (which require a normal CDF).

Remark 19. Proposition 18 holds for any choice of the basis functions $B_{i,j}(x,y)$. However, for the Taylor expansion basis of Example 3, Corollary 12 ensures that condition (25) is satisfied for any t small enough. Therefore the expansion (26) is convergent for short maturities.

We define the n-th order approximation of implied volatility as

$$\sigma^{(n)} := \sum_{h=0}^{n} \sigma_h. \tag{43}$$

For a given sequence of basis functions $(B_{i,j})$ explicit expressions for each σ_h in the sequence $(\sigma_h)_{h\geq 1}$ can be computed using a using a computer algebra program such as Wolfram's Mathematica. In Appendix C, we provide explicit expressions for σ_h for $h \leq 2$ when the basis functions are given by $B_{n,m}(x,y) = (x-\bar{x})^n(y-\bar{y})^m$ (as in Example 3). On the authors' websites, we also provide a Mathematica notebook which contains the expressions for σ_h for $h \leq 3$.

6 Implied volatility examples

In this Section we use the results of Section 5.2 to compute approximate model-induced implied volatilities (43) under five different model dynamics in which European option prices can be computed explicitly.

- Section 6.1: CEV local volatility model
- Section 6.2: Quadratic local volatility model
- Section 6.3: Heston stochastic volatility model
- Section 6.4: 3/2 stochastic volatility model
- Section 6.5: SABR local-stochastic volatility model

Assumption 20. In all of the examples that follow we assume basis functions $B_{n,h}(x,y) = (x-\bar{x})^n(y-\bar{y})^h$ (as in Example 3) with $(\bar{x},\bar{y}) = (X_0, Y_0)$. Thus, approximate implied volatilities can be computed using the formulas given in Appendix C as well as the Mathematica notebook available on the authors' websites.

6.1 CEV local volatility model

In the Constant Elasticity of Variance (CEV) local volatility model of Cox (1975), the dynamics of the underlying S are given by

$$\mathrm{d}S_t = \delta S_t^{\beta-1} S_t \mathrm{d}W_t, \qquad\qquad S_0 = s > 0.$$

The parameter β controls the relationship between volatility and price. When $\beta < 1$, volatility increases as $S \to 0^+$. This feature, referred to as the *leverage effect*, is commonly observed in equity markets. When $\beta < 1$, one also observes a negative at-the-money skew in the model-induced implied volatility surface. Like the leverage effect, a negative at-the-money skew is commonly observed in equity options markets. The origin is attainable when $\beta < 1$. In order to prevent the process S from taking negative values, one typically specifies zero as an absorbing boundary. Hence, the state space of S is $[0, \infty)$. In log notation $X := \log S$, we have the following dynamics [3]

$$\mathrm{d}X_t = -\frac{1}{2}\delta^2 \mathrm{e}^{2(\beta-1)X_t}\mathrm{d}t + \delta\,\mathrm{e}^{(\beta-1)X_t}\mathrm{d}W_t, \qquad\qquad X_0 = x := \log s. \qquad (44)$$

The generator of X is given by

$$\mathcal{A} = \frac{1}{2}\delta^2 \mathrm{e}^{2(\beta-1)x}(\partial_x^2 - \partial_x).$$

Thus, from (3) we identify

$$a(x,y) = \frac{1}{2}\delta^2 \mathrm{e}^{2(\beta-1)x}, \qquad b(x,y) = 0, \qquad c(x,y) = 0, \qquad \alpha(x,y) = 0.$$

We fix a time to maturity t and log-strike k. Using the formulas from Appendix C as well as the Mathematica notebook provided on the authors' websites, we compute explicitly

$$
\begin{aligned}
\sigma_0 &= \delta\,\mathrm{e}^{(\beta-1)x}, \\
\sigma_1 &= \frac{1}{2}(k-x)(\beta-1)\sigma_0, \\
\sigma_2 &= \frac{1}{96}(\beta-1)^2\sigma_0\left(8(k-x)^2 + t\sigma_{0,0}^2\left(4 - t\sigma_0^2\right)\right), \\
\sigma_3 &= -\frac{1}{192}t(k-x)(\beta-1)^3\sigma_0^3\left(-12 + 5t\sigma_0^2\right).
\end{aligned}
\qquad (45)
$$

In the CEV setting the exact price of a call option is derived in Cox (1975):

$$
\begin{aligned}
u(t,x) &= e^x Q(\kappa, 2 + \tfrac{2}{2-\beta}, 2\chi) - \mathrm{e}^k\left(1 - Q(2\chi, \tfrac{2}{2-\beta}, 2\kappa)\right), \\
Q(w,v,\mu) &= \sum_{n=0}^{\infty}\left(\frac{(\mu/2)^n \mathrm{e}^{-\mu/2}}{n!}\frac{\Gamma(v/2+n, w/2)}{\Gamma(v/2+n)}\right), \\
\chi &= \frac{2\mathrm{e}^{(2-\beta)x}}{\delta^2(2-\beta)^2 t}, \\
\kappa &= \frac{2\mathrm{e}^{(2-\beta)k}}{\delta^2(2-\beta)^2 t},
\end{aligned}
\qquad (46)
$$

---

[3] Here and in Section 6.2, we define $\log 0 := \lim_{x \searrow 0} \log x = -\infty$.

where $\Gamma(a)$ and $\Gamma(a, b)$ denote the complete and incomplete Gamma functions respectively. Thus, the exact implied volatility σ can be obtained by solving (23) numerically. In Figure 1 we plot our third order implied volatility approximation $\sigma^{(3)}$ and the exact implied volatility σ. For comparison, we also plot the implied volatility expansion of Hagan and Woodward (1999)

$$\sigma^{\text{HW}} = \frac{\delta}{f^{1-\beta}} \left(1 + \frac{(1-\beta)(2+\beta)}{24} \left(\frac{e^x - e^k}{f} \right)^2 + \frac{(1-\beta)^2}{24} \frac{\delta^2 t}{f^{2(1-\beta)}} + \cdots \right), \qquad f = \frac{1}{2}(e^x + e^k). \quad (47)$$

Relative errors of the two approximations are given in Figure 2. From the Figures, it is clear that our third order expansion $\sigma^{(3)}$ gives a better approximation of the true implied volatility than does the implied volatility expansion σ^{HW} of Hagan and Woodward (1999). The difference between $\sigma^{(3)}$ and σ^{HW} is most noticeable at strikes for which $|k - x| > 0.5$.

We are interested in finding the range of strikes and maturities over which our implied volatility expansion accurately approximates the exact implied volatility. Thus, in Figure 3 we provide a contour plot of the absolute value of the relative error $|\sigma^{(3)} - \sigma|/\sigma$ of our third order implied volatility approximation as a function of time to maturity t and log-moneyness $(k - x)$. From the Figure, we observe that the absolute value of the relative error of less than 0.3% for most options satisfying $(k - x) \in (-2.0, 2.0)$ and $t \in (0.0, 5.0)$ years.

6.2 Quadratic local volatility model

In the Quadratic local volatility model, the dynamics of the underlying S are given by

$$\text{d}S_t = \left(\frac{\delta}{S_t} \frac{(e^R - S_t)(e^L - S_t)}{e^R - e^L} \right) S_t \text{d}W_t, \qquad S_0 = s > 0, \qquad s < e^L < e^R.$$

Note that volatility increases as $S \to 0^+$, which is consistent with the leverage effect and which results in a negative at-the-money skew in the model-induced implied volatility surface. The left-hand root e^L of the polynomial $(e^R - s)(e^L - s)$ is an unattainable boundary for S. The origin, however, is attainable. In order to prevent the process S from taking negative values, one typically specifies zero as an absorbing boundary. Hence, the state space of S is $[0, e^L)$. In log notation $X := \log S$, we have the following dynamics

$$\text{d}X_t = -\frac{1}{2} \left(\frac{\delta}{e^{X_t}} \frac{(e^R - e^{X_t})(e^L - e^{X_t})}{e^R - e^L} \right)^2 \text{d}t + \frac{\delta}{e^{X_t}} \frac{(e^R - e^{X_t})(e^L - e^{X_t})}{e^R - e^L} \text{d}W_t, \qquad X_0 = x := \log s. \quad (48)$$

The generator of X is given by

$$\mathcal{A} = \frac{1}{2} \left(\frac{\delta}{e^x} \frac{(e^R - e^x)(e^L - e^x)}{e^R - e^L} \right)^2 (\partial_x^2 - \partial_x).$$

Thus, from (3) we identify

$$a(x, y) = \frac{1}{2} \left(\frac{\delta}{e^x} \frac{(e^R - e^x)(e^L - e^x)}{e^R - e^L} \right)^2, \qquad b(x, y) = 0, \qquad c(x, y) = 0, \qquad \alpha(x, y) = 0.$$

We fix a time to maturity t and log-strike k. Using the formulas from Appendix C, as well as the Mathematica notebook provided on the authors' websites we compute explicitly

$$\sigma_0 = \frac{\delta}{e^x} \frac{(e^R - e^x)(e^L - e^x)}{e^R - e^L},$$

$$\sigma_1 = \left(\frac{a_{1,0}}{2\sigma_0}\right)(k - x),$$

$$\sigma_2 = \left(-\frac{t\left(12 + t\sigma_0^2\right)a_{1,0}^2}{96\sigma_0} + \frac{1}{6}t\sigma_0 a_{2,0}\right) + \left(\frac{-3a_{1,0}^2 + 4\sigma_0^2 a_{2,0}}{12\sigma_0^3}\right)(k - x)^2, \qquad (49)$$

$$\sigma_3 = \frac{-t}{192\sigma_0^3}\left(\left(-12 + t\sigma_0^2\right)a_{1,0}^3 + 4\sigma_0^2\left(8 + t\sigma_0^2\right)a_{1,0}a_{2,0} - 48\sigma_0^4 a_{3,0}\right)(k - x)$$

$$+ \frac{1}{12\sigma_0^5}\left(3a_{1,0}^3 - 5\sigma_0^2 a_{1,0}a_{2,0} + 3\sigma_0^4 a_{3,0}\right)(k - x)^3,$$

where

$$a_{1,0} = \frac{\delta^2\left(-\sinh(L + R - 2x) + \sinh(L - x) + \sinh(R - x)\right)}{\cosh(L - R) - 1},$$

$$a_{2,0} = \frac{1}{4}\delta^2\left(2\cosh(L + R - 2x) - \cosh(L - x) - \cosh(R - x)\right)\operatorname{csch}^2\left(\frac{L - R}{2}\right),$$

$$a_{3,0} = \frac{e^{L+R}\delta^2\left(-4\sinh(L + R - 2x) + \sinh(L - x) + \sinh(R - x)\right)}{3\left(e^L - e^R\right)^2}.$$

The exact price of a call option is computed in Andersen (2011) Lemma 3.1. Assuming $k < L$ we have:

$$u(t, x) = e^{k_1}\mathcal{N}(-d_-^{(1)}) - e^{x_2}\mathcal{N}(d_+^{(2)}) - e^{x_1}\mathcal{N}(-d_+^{(1)}) + e^{k_2}\mathcal{N}(d_-^{(2)}), \qquad d_\pm^{(i)} = \frac{x_i - k_i \pm \frac{1}{2}\delta^2 t}{\sqrt{\delta^2 t}}, \qquad (50)$$

$$e^{k_1} = \frac{(e^L - e^k)(e^R - e^x)}{e^R - e^L}, \qquad\qquad e^{x_1} = \frac{(e^L - e^x)(e^R - e^k)}{e^R - e^L},$$

$$e^{k_2} = \frac{(e^R - e^k)(e^R - e^x)}{e^R - e^L}, \qquad\qquad e^{x_2} = \frac{(e^L - e^x)(e^L - e^k)}{e^R - e^L}.$$

Thus, the exact implied volatility σ can be obtained by solving (23) numerically.

In Figure 4 we plot our third order implied volatility approximation $\sigma^{(3)}$ and the exact implied volatility σ. Relative error of the approximation is given in Figure 5. In order to visualize the range of strikes and maturities over which our implied volatility expansion accurately approximates the exact implied volatility, we provide in Figure 6 a contour plot of the absolute value of the relative error $|\sigma^{(3)} - \sigma|/\sigma$ of our third order implied volatility approximation as a function of time to maturity t and log-moneyness $(k - x)$. From Figure 6, we observe a relative error of less than 1% for nearly all strikes k maturities t such that $(k - x) \in (-1.5, 1.5)$ and $t < 4$. A relative error of less than 3% is observed for nearly all strikes k maturities t such that $(k - x) \in (-1.5, 1.5)$ and $t < 10$.

6.3 Heston stochastic volatility model

Perhaps the most well-known stochastic volatility model is that of Heston (1993). In the Heston model, the dynamics of the underlying S are given by

$$dS_t = \sqrt{Z_t}S_t dW_t, \qquad\qquad\qquad S_0 = s > 0,$$

19

$$dZ_t = \kappa(\theta - Z_t)dt + \delta\sqrt{Z_t}dB_t, \qquad\qquad Z_0 = z > 0,$$
$$d\langle W, B\rangle_t = \rho\,dt.$$

Although it is not required, one typically sets $\rho < 0$ in order to capture the leverage effect. In log notation $(X, Y) := (\log S, \log Z)$ we have the following dynamics

$$dX_t = -\frac{1}{2}e^{Y_t}dt + e^{\frac{1}{2}Y_t}dW_t, \qquad\qquad X_0 = x := \log s,$$
$$dY_t = \left((\kappa\theta - \tfrac{1}{2}\delta^2)e^{-Y_t} - \kappa\right)dt + \delta\,e^{-\frac{1}{2}Y_t}dB_t, \quad Y_0 = y := \log z, \tag{51}$$
$$d\langle W, B\rangle_t = \rho\,dt.$$

The generator of (X, Y) is given by

$$\mathcal{A} = \frac{1}{2}e^y\left(\partial_x^2 - \partial_x\right) + \left((\kappa\theta - \tfrac{1}{2}\delta^2)e^{-y} - \kappa\right)\partial_y + \frac{1}{2}\delta^2 e^{-y}\partial_y^2 + \rho\,\delta\partial_x\partial_y.$$

Thus, using (3), we identify

$$a(x, y) = \frac{1}{2}e^y, \qquad b(x, y) = \frac{1}{2}\delta^2 e^{-y}, \qquad c(x, y) = \rho\,\delta, \qquad \alpha(x, y) = \left((\kappa\theta - \tfrac{1}{2}\delta^2)e^{-y} - \kappa\right).$$

We fix a time to maturity t and log-strike k. Using the formulas from Appendix C as well as the Mathematica notebook provided on the authors' websites, we compute explicitly

$$\sigma_0 = e^{y/2},$$
$$\sigma_1 = \frac{1}{8}e^{-y/2}t\left(-\delta^2 + 2\left(-e^y + \theta\right)\kappa + e^y\delta\rho\right) + \frac{1}{4}e^{-y/2}\delta\rho(k - x),$$
$$\sigma_2 = \left(\frac{-e^{-3y/2}}{128}t^2\left(\delta^2 - 2\theta\kappa\right)^2 + \frac{e^{y/2}}{96}t^2\left(5\kappa^2 - 5\delta\kappa\rho + \delta^2\left(-1 + 2\rho^2\right)\right)\right.$$
$$\left. + \frac{e^{-y/2}}{192}t\left(-4t\theta\kappa^2 - t\delta^3\rho + 2t\delta\theta\kappa\rho + 2\delta^2\left(8 + t\kappa + \rho^2\right)\right)\right)$$
$$+ \frac{1}{96}e^{-3y/2}t\delta\rho\left(5\delta^2 + 2\left(e^y - 5\theta\right)\kappa - e^y\delta\rho\right)(k - x) + \frac{1}{48}e^{-3y/2}\delta^2\left(2 - 5\rho^2\right)(k - x)^2,$$
$$\sigma_3 = \left(-\frac{e^{-5y/2}t^3\left(\delta^2 - 2\theta\kappa\right)^3}{1024} + \frac{e^{y/2}t^3(-2\kappa + \delta\rho)\left(6\kappa^2 - 6\delta\kappa\rho + \delta^2\left(-6 + 5\rho^2\right)\right)}{1536}\right. \tag{52}$$
$$+ \frac{e^{-3y/2}t^2\left(\delta^2 - 2\theta\kappa\right)\left(4t\theta\kappa^2 + t\delta^3\rho - 2t\delta\theta\kappa\rho + \delta^2\left(16 - 2t\kappa + 20\rho^2\right)\right)}{3072}$$
$$\left. + \frac{1}{768}e^{-y/2}t^2\left(3\delta^2\rho^2(-2\kappa + \delta\rho) + t\kappa\left(\delta^2 - 2\theta\kappa\right)(-\kappa + \delta\rho)\right)\right)$$
$$+ \left(\frac{7t^2\delta\rho e^{-5y/2}}{512}\left(\delta^2 - 2\theta\kappa\right)^2 + \frac{t^2\delta\rho e^{-y/2}}{384}\left(-3\kappa^2 + \delta\left(\delta + 3\kappa\rho - 2\delta\rho^2\right)\right)\right.$$
$$\left. - \frac{e^{-3y/2}}{768}t\delta\rho\left(20t\theta\kappa^2 + 5t\delta^3\rho - 10t\delta\theta\kappa\rho + 2\delta^2\left(8 - 5t\kappa + 9\rho^2\right)\right)\right)(k - x)$$
$$+ \frac{e^{-5y/2}t\delta^2}{384}\left(e^y(-2\kappa + \delta\rho)\left(-2 + 7\rho^2\right) - \left(\delta^2 - 2\theta\kappa\right)\left(-8 + 23\rho^2\right)\right)(k - x)^2$$
$$+ \frac{e^{-5y/2}\delta^3\rho}{96}\left(-5 + 8\rho^2\right)(k - x)^3.$$

The characteristic function of X_t is computed explicitly in Heston (1993)

$$\eta(t, x, y, \lambda) := \log\mathbb{E}_{x,y}e^{i\lambda X_t} = i\lambda x + C(t, \lambda) + D(t, \lambda)e^y,$$

20

$$C(t, \lambda) = \frac{\kappa\theta}{\delta^2} \left((\kappa - \rho\delta\mathtt{i}\lambda + d(\lambda))t - 2\log\left[\frac{1 - f(\lambda)\mathrm{e}^{d(\lambda)t}}{1 - f(\lambda)} \right] \right),$$

$$D(t, \lambda) = \frac{\kappa - \rho\delta\mathtt{i}\lambda + d(\lambda)}{\delta^2} \frac{1 - \mathrm{e}^{d(\lambda)t}}{1 - f(\lambda)\mathrm{e}^{d(\lambda)t}},$$

$$f(\lambda) = \frac{\kappa - \rho\delta\mathtt{i}\lambda + d(\lambda)}{\kappa - \rho\delta\mathtt{i}\lambda - d(\lambda)},$$

$$d(\lambda) = \sqrt{\delta^2(\lambda^2 + \mathtt{i}\lambda) + (\kappa - \rho\mathtt{i}\lambda\delta)^2}.$$

Thus, the price of a European call option can be computed using standard Fourier methods

$$u(t, x, y) = \frac{1}{2\pi}\int_{\mathbb{R}} \mathrm{d}\lambda_r\, \mathrm{e}^{\eta(t,x,y,\lambda)}\widehat{h}(\lambda), \qquad \widehat{h}(\lambda) = \frac{-\mathrm{e}^{k-\mathtt{i}k\lambda}}{\mathtt{i}\lambda + \lambda^2}, \qquad \lambda = \lambda_r + \mathtt{i}\lambda_i, \qquad \lambda_i < -1. \quad (53)$$

Note, since the call option payoff $h(x) = (\mathrm{e}^x - \mathrm{e}^k)^+$ is not in $L^1(\mathbb{R})$, its Fourier transform $\widehat{h}(\lambda)$ must be computed in a generalized sense by fixing an imaginary component of the Fourier variable $\lambda_i < -1$. Using (53) the exact implied volatility σ can be computed to solving (23) numerically. In Figure 7 we plot our third order implied volatility approximation $\sigma^{(3)}$ and the exact implied volatility σ. For comparison, we also plot the small-time near-the-money implied volatility expansion of Forde, Jacquier, and Lee (2012) (see Theorem 3.2 and Corollary 4.3)

$$\sigma^{\mathrm{FJL}} = \left(g_0^2 + g_1\, t + o(t) \right)^{1/2}, \tag{54}$$

$$g_0 = \mathrm{e}^{y/2}\left(1 + \frac{1}{4}\rho\delta(k - x)\mathrm{e}^{-y} + \frac{1}{24}\left(1 - \frac{5\rho^2}{2} \right)\delta^2(k - x)^2\mathrm{e}^{-2y} \right) + \mathcal{O}((k - x)^3),$$

$$g_1 = -\frac{\delta^2}{12}\left(1 - \frac{\rho^2}{4} \right) + \frac{\mathrm{e}^y\rho\delta}{4} + \frac{\kappa}{2}(\theta - \mathrm{e}^y) + \frac{1}{24}\rho\delta\mathrm{e}^{-y}(\delta^2\overline{\rho}^2 - 2\kappa(\theta + \mathrm{e}^y) + \rho\delta\mathrm{e}^y)(k - x)$$

$$\qquad + \frac{\delta^2\mathrm{e}^{-2y}}{7680}\left(176\delta^2 - 480\kappa\theta - 712\rho^2\delta^2 + 521\rho^4\delta^2 + 40\rho^3\delta\mathrm{e}^y + 1040\kappa\theta\rho^2 - 80\kappa\rho^2\mathrm{e}^y \right)(k - x)^2$$

$$\qquad + \mathcal{O}((k - x)^3), \qquad \overline{\rho} = \sqrt{1 - \rho^2}.$$

Relative errors of the two approximations are given in Figure 8. It is clear from the Figures that our third order implied volatility expansions $\sigma^{(3)}$ provides a better approximation of the true implied volatility σ than does the implied volatility expansion σ^{FJL}. The improvement marked by $\sigma^{(3)}$ is particularly noticeable at the largest strikes and at longer maturities.

We are interested in learning the range of strikes and maturities over which our implied volatility expansion accurately approximates the exact implied volatility. Thus, in Figure 9 we provide a contour plot of the absolute value of the relative error $|\sigma^{(3)} - \sigma|/\sigma$ of our third order implied volatility approximation as a function of time to maturity t and log-moneyness $(k - x)$. From the Figure, we observe an absolute relative error of less than 2% for most options satisfying $(k - x) \in (-0.75, 0.75)$ and $t \in (0.0, 2.7)$ years.

6.4   3/2 stochastic volatility model

We consider now the 3/2 stochastic volatility model. The risk-neutral dynamics of the underlying S in this setting are given by

$$\mathrm{d}S_t = \sqrt{Z_t}S_t\mathrm{d}W_t, \qquad\qquad\qquad S_0 = s > 0,$$

$$dZ_t = Z_t \left(\kappa(\theta - Z_t)dt + \delta\sqrt{Z_t}dB_t \right), \qquad\qquad Z_0 = z > 0,$$

$$d\langle W, B \rangle_t = \rho\, dt.$$

As in all stochastic volatility models, one typically sets $\rho < 0$ in order to capture the leverage effect. The $3/2$ model is noteworthy in that it does not fall into the affine class of Duffie, Pan, and Singleton (2000), and yet it still allows for European option prices to be computed in semi-closed form (as a Fourier integral). Notice however that the characteristic function (given in (57) below) involves special functions such as the Gamma and the confluent hypergeometric functions. Therefore, Fourier pricing methods are not an efficient means of computed prices. The importance of the $3/2$ model in the pricing of options on realized variance is well documented by Drimus (2012). In particular, the $3/2$ model allows for upward-sloping implied volatility of variance smiles while Heston's model leads to downward-sloping volatility of variance smiles, in disagreement with observed skews in variance markets.

In log notation $(X, Y) := (\log S, \log Z)$ we have the following dynamics

$$dX_t = -\frac{1}{2}e^{Y_t}dt + e^{\frac{1}{2}Y_t}dW_t, \qquad\qquad X_0 = x := \log s,$$

$$dY_t = \left(\kappa(\theta - e^{Y_t}) - \frac{1}{2}\delta^2 e^{Y_t} \right) dt + \delta\, e^{\frac{1}{2}Y_t}dB_t, \quad Y_0 = y := \log z, \qquad (55)$$

$$d\langle W, B \rangle_t = \rho\, dt.$$

The generator of (X, Y) is given by

$$\mathcal{A} = \frac{1}{2}e^y \left(\partial_x^2 - \partial_x \right) + \left(\kappa(\theta - e^y) - \frac{1}{2}\delta^2 e^y \right) \partial_y + \frac{1}{2}\delta^2 e^y \partial_y^2 + \rho\,\delta\, e^y \partial_x \partial_y.$$

Thus, using (3), we identify

$$a(x, y) = \frac{1}{2}e^y, \qquad b(x, y) = \frac{1}{2}\delta^2 e^y, \qquad c(x, y) = \rho\,\delta\, e^y, \qquad \alpha(x, y) = \kappa(\theta - e^y) - \frac{1}{2}\delta^2 e^y.$$

We fix a time to maturity t and log-strike k. Using the formulas from Appendix C as well as the Mathematica notebook provided on the authors' websites, we compute explicitly

$$\sigma_0 = e^{y/2},$$

$$\sigma_1 = -\frac{1}{8}e^{y/2}t \left(-2\theta\kappa + e^y \left(\delta^2 + 2\kappa - \delta\rho \right) \right) + \frac{1}{4}e^{y/2}\delta\rho(k - x),$$

$$\sigma_2 = e^{y/2}\left(\frac{5}{96}t^2\theta^2\kappa^2 \right) + e^{3y/2}\left(-\frac{1}{96}t \left(18t\theta\kappa^2 - 9t\delta\theta\kappa\rho + \delta^2 \left(-8 + 9t\theta\kappa + 7\rho^2 \right) \right) \right)$$

$$\qquad + e^{6y/2}\left(\frac{1}{384}t^2 \left(13\delta^4 + 52\kappa^2 - 26\delta^3\rho - 52\delta\kappa\rho + 4\delta^2 \left(-1 + 13\kappa + 4\rho^2 \right) \right) \right)$$

$$\qquad + \frac{1}{96}e^{y/2}t\delta\rho \left(6\theta\kappa - 7e^y \left(\delta^2 + 2\kappa - \delta\rho \right) \right)(k - x) - \frac{1}{48}e^{y/2}\delta^2 \left(-2 + \rho^2 \right)(k - x)^2, \qquad (56)$$

$$\sigma_3 = \frac{1}{3072}\left(e^{y/2}\left(24t^3\theta^3\kappa^3 \right) + e^{3y/2}\left(-12t^2\theta\kappa \left(22t\theta\kappa^2 - 11t\delta\theta\kappa\rho + \delta^2 \left(-16 + 11t\theta\kappa + 14\rho^2 \right) \right) \right) \right.$$

$$\qquad + e^{5y/2}\left(-240t^2\delta^4 - 480t^2\delta^2\kappa - 40t^3\delta^2\theta\kappa + 130t^3\delta^4\theta\kappa + 520t^3\delta^2\theta\kappa^2 + 520t^3\theta\kappa^3 + 240t^2\delta^3\rho \right.$$

$$\qquad \left. \left. - 260t^3\delta^3\theta\kappa\rho - 520t^3\delta\theta\kappa^2\rho + 180t^2\delta^4\rho^2 + 360t^2\delta^2\kappa\rho^2 + 160t^3\delta^2\theta\kappa\rho^2 - 180t^2\delta^3\rho^3 \right) \right)$$

$$+ e^{7y/2} \left(-t^3 \left(\delta^2 + 2\kappa - \delta\rho\right) \left(35\delta^4 + 140\kappa^2 - 70\delta^3\rho - 140\delta\kappa\rho + 2\delta^2 \left(-16 + 70\kappa + 29\rho^2\right)\right)\right) \Big)$$

$$+ \frac{1}{1536} \Big(e^{y/2} \left(20t^2\delta\theta^2\kappa^2\rho\right) + e^{3y/2} \left(-12t\delta\rho \left(14t\theta\kappa^2 - 7t\delta\theta\kappa\rho + \delta^2 \left(-4 + 7t\theta\kappa + 3\rho^2\right)\right)\right)$$

$$+ e^{5y/2} \left(t^2\delta\rho \left(45\delta^4 + 180\kappa^2 - 90\delta^3\rho - 180\delta\kappa\rho + 4\delta^2 \left(-4 + 45\kappa + 14\rho^2\right)\right)\right) \Big) \Big)(k - x)$$

$$+ \frac{1}{384} e^{y/2} t\delta^2 \left(e^y \left(\delta^2 + 2\kappa - \delta\rho\right) \left(-8 + \rho^2\right) - 2\theta\kappa \left(-2 + \rho^2\right)\right)(k - x)^2.$$

To the best of our knowledge, the above formula is the first explicit implied volatility expansion for the 3/2 model. The characteristic function of X_t is given, for example, in Proposition 3.2 of Baldeaux and Badran (2012). We have

$$\mathbb{E}_{x,y} e^{\mathrm{i}\lambda X_t} = e^{\mathrm{i}\lambda x} \frac{\Gamma(\gamma - \alpha)}{\Gamma(\gamma)} \left(\frac{2}{\delta^2 z}\right)^\alpha M\left(\alpha, \gamma, \frac{-2}{\delta^2 z}\right), \qquad z = \frac{e^y}{\kappa\theta}(e^{\kappa\theta t} - 1), \qquad \gamma = 2\left(\alpha + 1 - \frac{p}{\delta^2}\right), \quad (57)$$

$$\alpha = -\left(\frac{1}{2} - \frac{p}{\delta^2}\right) + \left(\left(\frac{1}{2} - \frac{p}{\delta^2}\right)^2 + 2\frac{q}{\delta^2}\right)^{1/2}, \qquad p = -\kappa + \mathrm{i}\delta\rho\lambda, \qquad q = \frac{1}{2}(\mathrm{i}\lambda + \lambda^2),$$

where Γ is a Gamma function and M is a confluent hypergeometric function. Thus, the price of a European call option can be computed using standard Fourier methods

$$u(t, x, y) = \frac{1}{2\pi} \int_\mathbb{R} \mathrm{d}\lambda_r \, \widehat{h}(\lambda) \mathbb{E}_{x,y} e^{\mathrm{i}\lambda X_t}, \qquad\qquad \lambda = \lambda_r + \mathrm{i}\lambda_i, \qquad\qquad \lambda_i < -1, \qquad (58)$$

where $\widehat{h}(\lambda)$ is given in (53). Using (58) the exact implied volatility σ can be computed to solving (23) numerically.

In Figure 10 we plot our third order implied volatility approximation $\sigma^{(3)}$ and the exact implied volatility σ. Relative error of the approximation is given in Figure 11. In order to visualize the range of strikes and maturities over which our implied volatility expansion accurately approximates the exact implied volatility, we provide in Figure 12 a contour plot of the absolute value of the relative error $|\sigma^{(3)} - \sigma|/\sigma$ of our third order implied volatility approximation as a function of time to maturity t and log-moneyness $(k-x)$. From Figures 12, we observe a relative error of less than 1% for nearly all strikes k maturities t such that $(k-x) \in (-1.0, 0.8)$ and $t < 1.5$ years. A relative error of less than 3% is observed for nearly all strikes k maturities t such that $(k - x) \in (-1.0, 0.8)$ and $t < 2.5$ years.

6.5   SABR local-stochastic volatility

The SABR model of Hagan, Kumar, Lesniewski, and Woodward (2002) is a local-stochastic volatility model in which the risk-neutral dynamics of S are given by

$$\mathrm{d}S_t = Z_t S_t^\beta \mathrm{d}W_t, \qquad\qquad S_0 = s > 0,$$
$$\mathrm{d}Z_t = \delta Z_t \mathrm{d}B_t, \qquad\qquad Z_0 = z > 0,$$
$$\mathrm{d}\langle W, B \rangle_t = \rho \, \mathrm{d}t.$$

Modeling the non-local component of volatility Z as a geometric Brownian motion results in a true implied volatility smile (i.e., upward sloping implied volatility for high strikes); this is in contrast to the CEV

model, for which the model-induced implied volatility is monotone decreasing (for $\beta < 1$). In log notation $(X, Y) := (\log S, \log Z)$ we have, we have the following dynamics:

$$
\begin{aligned}
\mathrm{d}X_t &= -\frac{1}{2}\mathrm{e}^{2Y_t + 2(\beta-1)X_t}\mathrm{d}t + \mathrm{e}^{Y_t + (\beta-1)X_t}\mathrm{d}W_t, \quad X_0 = x := \log s, \\
\mathrm{d}Y_t &= -\frac{1}{2}\delta^2\mathrm{d}t + \delta\,\mathrm{d}B_t, \qquad\qquad\qquad\qquad\quad Y_0 = y := \log z, \\
\mathrm{d}\langle W, B\rangle_t &= \rho\,\mathrm{d}t.
\end{aligned}
\tag{59}
$$

The generator of (X, Y) is given by

$$
\mathcal{A} = \frac{1}{2}\mathrm{e}^{2y + 2(\beta-1)x}(\partial_x^2 - \partial_x) - \frac{1}{2}\delta^2\partial_y + \frac{1}{2}\delta^2\partial_y^2 + \rho\,\delta\,\mathrm{e}^{y + (\beta-1)x}\partial_x\partial_y.
$$

Thus, using (3), we identify

$$
a(x, y) = \frac{1}{2}\mathrm{e}^{2y + 2(\beta-1)x}, \qquad b(x, y) = \frac{1}{2}\delta^2, \qquad c(x, y) = \rho\,\delta\,\mathrm{e}^{y + (\beta-1)x}, \qquad \alpha(x, y) = -\frac{1}{2}\delta^2.
$$

We fix a time to maturity t and log-strike k. Using the formulas from Appendix C as well as the Mathematica notebook provided on the authors' websites, we compute explicitly

$$
\sigma_0 = \mathrm{e}^{y + (\beta-1)x}, \qquad \sigma_1 = \sigma_{1,0} + \sigma_{0,1}, \qquad \sigma_2 = \sigma_{2,0} + \sigma_{1,1} + \sigma_{0,1}, \qquad \sigma_3 = \sigma_{3,0} + \sigma_{2,1} + \sigma_{1,2} + \sigma_{0,3}, \tag{60}
$$

where

$$
\sigma_{1,0} = \frac{1}{2}(k - x)(-1 + \beta)\sigma_0,
$$

$$
\sigma_{0,1} = \frac{1}{4}\delta\left(2(k - x)\rho + t\sigma_0\left(-\delta + \rho\sigma_0\right)\right),
$$

$$
\sigma_{2,0} = \frac{1}{96}(-1 + \beta)^2\sigma_0\left(8(k - x)^2 + t\sigma_0^2\left(4 - t\sigma_0^2\right)\right),
$$

$$
\sigma_{1,1} = -\frac{1}{48}t(-1 + \beta)\delta\sigma_0\left(6(k - x)\delta - 2(6 + 5k - 5x)\rho\sigma_0 + t\rho\sigma_0^3\right),
$$

$$
\sigma_{0,2} = \frac{1}{96}t\delta^2\sigma_0\left(32 + 5t\delta^2 - 12\rho^2 + 2t\sigma_0\left(-7\delta\rho + \left(-2 + 6\rho^2\right)\sigma_0\right)\right)
$$

$$
\qquad - \frac{1}{24}t\delta^2\rho\left(\delta - 3\rho\sigma_0\right)(k - x) + \frac{\delta^2\left(2 - 3\rho^2\right)}{12\sigma_0}(k - x)^2,
$$

$$
\sigma_{3,0} = -\frac{1}{192}t(k - x)(-1 + \beta)^3\sigma_0^3\left(-12 + 5t\sigma_0^2\right),
$$

$$
\sigma_{2,1} = \frac{1}{384}t^2(-1 + \beta)^2\delta\sigma_0^3\left(-12\delta + 28\rho\sigma_0 + t\sigma_0^2\left(5\delta - 7\rho\sigma_0\right)\right)
$$

$$
\qquad - \frac{13}{192}t(-1 + \beta)^2\delta\rho\sigma_0^2\left(-4 + t\sigma_0^2\right)(k - x) - \frac{1}{48}t(-1 + \beta)^2\delta\sigma_0\left(\delta - 3\rho\sigma_0\right)(k - x)^2,
$$

$$
\sigma_{1,2} = \frac{1}{192}t^2(-1 + \beta)\delta^2\rho\sigma_0^2\left(-28\delta + 52\rho\sigma_0 + t\sigma_0^2\left(5\delta - 7\rho\sigma_0\right)\right)
$$

$$
\qquad + \frac{1}{192}t(-1 + \beta)\delta^2\sigma_0\left(32 + 5t\delta^2 + 12\rho^2 - 22t\delta\rho\sigma_0 + 4t\left(-3 + 5\rho^2\right)\sigma_0^2\right)(k - x)
$$

$$
\qquad + \frac{1}{24}t(-1 + \beta)\delta^2\rho^2\sigma_0(k - x)^2 + \frac{(-1 + \beta)\delta^2\left(-2 + 3\rho^2\right)}{24\sigma_0}(k - x)^3,
$$

$$
\sigma_{0,3} = -\sigma_0\frac{1}{128}t^2\delta^4\left(16 + t\delta^2 - 4\rho^2\right) + \sigma_0^2\frac{1}{384}t^2\delta^3\rho\left(104 + 19t\delta^2 - 36\rho^2\right)
$$

$$+ \sigma_0^3 \frac{1}{192} t^3 \delta^4 \left(8 - 21\rho^2\right) + \sigma_0^4 \frac{1}{192} t^3 \delta^3 \rho \left(-11 + 15\rho^2\right)$$

$$- \frac{1}{192} t \delta^3 \rho \left(8 + 12x + t\delta^2 - 12\rho^2 + 6t\sigma_0 \left(\delta\rho + \left(1 - 2\rho^2\right)\sigma_0\right)\right)(k - x)$$

$$- \frac{1}{16} t \delta^3 \rho \left(-1 + \rho^2\right)(k - x)^2 + \frac{\delta^3 \rho \left(-5 + 6\rho^2\right)}{24\sigma_0^2}(k - x)^3.$$

There is no formula for European option prices in the general SABR setting. However, for the special zero-correlation case $\rho = 0$ the exact price of a European call is computed in Antonov and Spector (2012):

$$u(t, x) = e^{(x+k)/2} \frac{e^{-\delta^2 t/8}}{\sqrt{2\pi\delta^2 t}} \left\{ \frac{1}{\pi} \int_0^\infty dV \int_0^\pi d\phi \frac{1}{V} \left(\frac{V}{V_0}\right)^{-1/2} \frac{\sin\phi \sin(|\nu|\phi)}{b - \cos\phi} \exp\left(\frac{\xi_\phi^2}{2\delta^2 t}\right) \right.$$

$$\left. + \frac{\sin(|\nu|\pi)}{\pi} \int_0^\infty dV \int_0^\infty d\psi \frac{1}{V} \left(\frac{V}{V_0}\right)^{-1/2} \frac{\sinh\psi}{b - \cosh\psi} e^{-|\nu|\psi} \exp\left(\frac{\xi_\psi^2}{2\delta^2 t}\right) \right\} + (e^x - e^k)^+,$$

$$\xi_\phi = \arccos\left(\frac{q_h^2 + q_x^2 + V^2 + V_0^2}{2VV_0} - \frac{q_h q_x}{VV_0} \cos\phi\right),$$

$$\xi_\psi = \arccos\left(\frac{q_h^2 + q_x^2 + V^2 + V_0^2}{2VV_0} + \frac{q_h q_x}{VV_0} \cosh\psi\right),$$

$$b = \frac{q_h^2 + q_x^2}{2q_h q_x}, \qquad q_h = \frac{e^{(1-\beta)k}}{1-\beta}, \qquad q_x = \frac{e^{(1-\beta)x}}{1-\beta}, \qquad \nu = \frac{-1}{2(1-\beta)}, \qquad V_0 = \frac{e^y}{\delta}.$$

$$(61)$$

Thus, in the zero-correlation setting, the exact implied volatility σ can be obtained by using the above formula and then by solving (23) numerically. In Figure 13 we plot our third order implied volatility approximation $\sigma^{(3)}$ and the exact implied volatility σ. For comparison, we also plot the implied volatility expansion of Hagan, Kumar, Lesniewski, and Woodward (2002)

$$\sigma^{\text{HKLW}} = \delta \frac{x - k}{D(\zeta)} \left\{ 1 + t\delta^2 \left[\frac{2\gamma_2 - \gamma_1^2 + 1/f^2}{24} \left(\frac{e^{y+\beta f}}{\delta}\right)^2 + \frac{\rho\gamma_1 e^{y+\beta f}}{4\delta} + \frac{2 - 3\rho^2}{24} \right] \right\}, \qquad (62)$$

$$f = \frac{1}{2}(e^x + e^k),$$

$$\zeta = \frac{\delta e^{-y}}{\beta - 1} \left(e^{(1-\beta)k} - e^{(1-\beta)x}\right),$$

$$\gamma_1 = \beta/f,$$

$$\gamma_2 = \beta(\beta - 1)/f^2,$$

$$D(\zeta) = \log\left(\frac{\sqrt{1 - 2\rho\zeta + \zeta^2} + \zeta - \rho}{1 - \rho}\right).$$

Note that we use the "corrected" SABR formula, which appears in Obloj (2008). Relative errors of the two approximations are given in Figure 14. From the Figures we observe that both expansions $\sigma^{(3)}$ and σ^{HKLW} provide excellent approximations of the true implied volatility σ for options with maturities of ~ 1.5 years or less. However, for longer maturities $t > 2.0$, it is clear that $\sigma^{(3)}$ more closely approximates σ than does σ^{HKLW}.

We are interested in learning the range of strikes and maturities over which our implied volatility expansion accurately approximates the exact implied volatility. Thus, in Figure 15 we provide a contour plot of

the absolute value of the relative error $|\sigma^{(3)} - \sigma|/\sigma$ of our third order implied volatility approximation as a function of time to maturity t and log-moneyness $(k - x)$. From the Figure, we observe an absolute relative error of less than 2% for most options satisfying $(k - x) \in (-1.5, 1.4)$ and $t < 5.0$ years.

7 Conclusions and future work

In this paper we consider general local-stochastic volatility models. In this setting, we provide a family of approximations – one for each choice of the basis functions (i.e. Taylor series, Two-point Taylor series, L^2 basis, etc.) – for (i) the transition density of the underlying (ii) European-style option prices and (iii) implied volatilities. Our density expansions require no integration; every term can be written as a sum of Hermite polynomials multiplied by a Gaussian density. The terms in our option price expansions are expressed as a differential operator acting on the Black-Scholes price. Thus, to compute approximate prices, one requires only a normal CDF. Our implied volatility expansion is explicit; it requires no special functions nor does it require any numerical integration. Thus, approximate implied volatilities can be computed even faster than option prices.

We carry out extensive computations using the Taylor series basis functions. In particular, we establish the rigorous error bounds of our transition density expansion. We also implement our implied volatility approximation under five separate model dynamics: CEV local volatility, Quadratic local volatility, Heston stochastic volatility, 3/2 stochastic volatility, and SABR local-stochastic volatility. In each setting we demonstrate that our implied volatility expansion provides an excellent approximation of the true implied volatility over a large range of strikes and maturities.

Looking forward, we are currently working to extend our density, pricing and implied volatility approximations to Lévy-type local-stochastic volatility models. We are also examining how our approximation techniques can be applied to a variety of exotic options. Finally, we are investigating how different basis functions can be used advantageously in different settings.

A Proof of Proposition 7

The formal adjoint of an operator $\mathcal{A}$ in $L^2(\mathbb{R}^2, \mathrm{d}x\mathrm{d}y)$ is the operator $\mathcal{A}^\dagger$ such that

$$\langle f, \mathcal{A}g \rangle = \langle \mathcal{A}^\dagger f, g \rangle, \qquad \langle u, v \rangle := \int_{\mathbb{R}^2} \mathrm{d}x\mathrm{d}y\, \overline{u(x,y)} v(x,y), \qquad u, v \in \mathcal{S}(\mathbb{R}^2).$$

Observe that

$$\mathcal{A}_h^\dagger = \sum_{l=0}^{h} \phi_{h-l,l}(\mathcal{D}_x, \mathcal{D}_y) B_{h-l,l}(x, y),$$

which can be deduced by integrating by parts. Now, we note that

$$\langle \psi_{\lambda,\omega}, \mathcal{A}_h u(t, \cdot, \cdot) \rangle = \langle \mathcal{A}_h^\dagger \psi_{\lambda,\omega}, u \rangle$$

$$= \sum_{l=0}^{h} \langle \phi_{h-l,l}(\mathcal{D}_x, \mathcal{D}_y) B_{h-l,l} \psi_{\lambda,\omega}, u(t, \cdot, \cdot) \rangle$$

26

$$= \sum_{l=0}^{h} B_{h-l,l}(\mathtt{i}\partial_\lambda, \mathtt{i}\partial_\omega)\phi_{h-l,l}(\lambda,\omega)\langle\psi_{\lambda,\omega}, u(t,\cdot,\cdot)\rangle$$

$$= \sum_{l=0}^{h} B_{h-l,l}(\mathtt{i}\partial_\lambda, \mathtt{i}\partial_\omega)\phi_{h-l,l}(\lambda,\omega)\widehat{u}(t,\lambda,\omega).$$

We Fourier transform equation (15). Focusing first on the left-hand side, and using the above result we have

$$\langle\psi_{\lambda,\omega}, (-\partial_t + \mathcal{A}_0)u_n(t,\cdot,\cdot)\rangle = -\partial_t\langle\psi_{\lambda,\omega}, u_n(t,\cdot,\cdot)\rangle + \langle\mathcal{A}_0^\dagger\psi_{\lambda,\omega}, u_n(t,\cdot,\cdot)\rangle = (-\partial_t + \phi_{0,0}(\lambda,\omega))\,\widehat{u}_n(t,\lambda,\omega).$$

Next, for the right-hand side of (15) we compute

$$-\sum_{h=1}^{n}\langle\psi_{\lambda,\omega}, \mathcal{A}_h u_{n-h}(t,\cdot,\cdot)\rangle = -\sum_{h=1}^{n}\sum_{l=0}^{h} B_{h-l,l}(\mathtt{i}\partial_\lambda, \mathtt{i}\partial_\omega)\phi_{h-l,l}(\lambda,\omega)\widehat{u}_{n-h}(t,\lambda,\omega).$$

Thus, we have the following ODE (in t) for $\widehat{u}_0(t,\lambda,\omega)$

$$(-\partial_t + \phi_{0,0}(\lambda,\omega))\,\widehat{u}_0(t,\lambda,\omega) = 0, \qquad\qquad \widehat{u}_0(0,\lambda,\omega) = \widehat{H}(\lambda,\omega). \qquad (63)$$

Likewise, for $\widehat{u}_n(t,\lambda,\omega)$ we have the following ODE in t

$$\left.\begin{aligned} (-\partial_t + \phi_{0,0}(\lambda,\omega))\,\widehat{u}_n(t,\lambda,\omega) &= -\sum_{h=1}^{n}\sum_{l=0}^{h} B_{h-l,l}(\mathtt{i}\partial_\lambda, \mathtt{i}\partial_\omega)\phi_{h-l,l}(\lambda,\omega)\widehat{u}_{n-h}(t,\lambda,\omega), \\ \widehat{u}_n(0,\lambda,\omega) &= 0. \end{aligned}\right\} \quad n \geq 1. \qquad (64)$$

The solutions of (63) and (64) are given by (17) and (18) respectively.

B Proof of Theorem 9

Throughout this Appendix, we shall use the following identity repeatedly:

$$\widehat{u}_0(s,\lambda,\omega) = \mathrm{e}^{\mathtt{i}\lambda x + \mathtt{i}\omega y}\widehat{u}_0(t,\lambda,\omega)\frac{1}{\mathrm{e}^{\mathtt{i}\lambda x + \mathtt{i}\omega y + (t-s)\phi_{0,0}}}. \qquad (65)$$

We begin by computing $u_1(t,x,y)$. We have

$$u_1(t,x,y)$$

$$\overset{1}{=} \frac{1}{2\pi}\int_{\mathbb{R}^2}\mathrm{d}\lambda\mathrm{d}\omega\,\mathrm{e}^{\mathtt{i}\lambda x + \mathtt{i}\omega y}\,\widehat{u}_1(t,\lambda,\omega)$$

$$\overset{2}{=} \frac{1}{2\pi}\int_{\mathbb{R}^2}\mathrm{d}\lambda\mathrm{d}\omega\int_0^t\mathrm{d}s\sum_{i=0}^{1}\mathrm{e}^{\mathtt{i}\lambda x + \mathtt{i}\omega y + (t-s)\phi_0(\lambda,\omega)}B_{1-i,i}(\mathtt{i}\partial_\lambda, \mathtt{i}\partial_\omega)\phi_{1-i,i}(\lambda,\omega)\widehat{u}_0(s,\lambda,\omega)$$

$$\overset{3}{=} \frac{1}{2\pi}\int_{\mathbb{R}^2}\mathrm{d}\lambda\mathrm{d}\omega\int_0^t\mathrm{d}s\sum_{i=0}^{1}\widehat{u}_0(s,\lambda,\omega)\phi_{1-i,i}(\lambda,\omega)B_{1-i,i}(-\mathtt{i}\partial_\lambda, -\mathtt{i}\partial_\omega)\mathrm{e}^{\mathtt{i}\lambda x + \mathtt{i}\omega y + (t-s)\phi_{0,0}(\lambda,\omega)}$$

$$\overset{4}{=} \frac{1}{2\pi}\int_{\mathbb{R}^2}\mathrm{d}\lambda\mathrm{d}\omega\,\mathrm{e}^{\mathtt{i}\lambda x + \mathtt{i}\omega y}\widehat{u}_0(t,\lambda,\omega)\int_0^t\mathrm{d}s\sum_{i=0}^{1}\phi_{1-i,i}(\lambda,\omega)\frac{B_{1-i,i}(-\mathtt{i}\partial_\lambda, -\mathtt{i}\partial_\omega)\mathrm{e}^{\mathtt{i}\lambda x + \mathtt{i}\omega y + (t-s)\phi_{0,0}(\lambda,\omega)}}{\mathrm{e}^{\mathtt{i}\lambda x + \mathtt{i}\omega y + (t-s)\phi_{0,0}(\lambda,\omega)}}$$

$$\overset{5}{=} \frac{1}{2\pi} \int_{\mathbb{R}^2} \mathrm{d}\lambda \mathrm{d}\omega \, \mathrm{e}^{\mathrm{i}\lambda x + \mathrm{i}\omega y} \widehat{u}_0(t,\lambda,\omega) \int_0^t \mathrm{d}s \, \Phi_1(s,t,x,y,\lambda,\omega,-\mathrm{i}\partial_\lambda,-\mathrm{i}\partial_\omega)$$

$$\overset{6}{=} \frac{1}{2\pi} \int_{\mathbb{R}^2} \mathrm{d}\lambda \mathrm{d}\omega \, \mathrm{e}^{\mathrm{i}\lambda x + \mathrm{i}\omega y} \widehat{u}_0(t,\lambda,\omega) \mathcal{L}_1(t,x,y,\lambda,\omega)$$

$$\overset{7}{=} \mathcal{L}_1(t,x,y,\mathcal{D}_x,\mathcal{D}_y) u_0(t,x,y),$$

where $\mathcal{L}_1(t,x,y,\lambda,\omega)$ is given in (19). Because we shall repeat the above steps for higher order terms, we describe the above computation in detail. In the first equality we have expressed u_1 as an inverse Fourier transform of $\widehat{u}_1$. In the second equality we have used Proposition 7 to write out $\widehat{u}_1$ explicitly. In the third equality we have used integration by parts to replace $B_{1-i,i}(\mathrm{i}\partial_\lambda,\mathrm{i}\partial_\omega)$ acting on $\phi_{1-i,i}(\lambda,\omega)\widehat{u}_0(s,\lambda,\omega)$ by its adjoint $B_{1-i,i}(-\mathrm{i}\partial_\lambda,-\mathrm{i}\partial_\omega)$ acting on $\mathrm{e}^{\mathrm{i}\lambda x + \mathrm{i}\omega y + (t-s)\phi_{0,0}(\lambda,\omega)}$. In the fourth equality we have used (65). In the fifth equality we have used (20) to recognize the inner-most integrand as $\Phi_1(s,t,x,y,\lambda,\omega,-\mathrm{i}\partial_\lambda,-\mathrm{i}\partial_\omega)$. In the sixth step we have used (19) to recognize the inner-most integral as $\mathcal{L}_1(s,t,x,y,\lambda,\omega)$. Lastly, in the seventh equality, we have used (5) and the fact that $\mathcal{L}_1(s,t,x,y,\lambda,\omega)$ is the symbol of the differential operator $\mathcal{L}_{1,0}(s,t,x,y,\mathcal{D}_x,\mathcal{D}_y)$.

Now, we move on to $u_2(t,x,y)$. We have

$$u_2(t,x,y)$$

$$= \frac{1}{2\pi} \int_{\mathbb{R}^2} \mathrm{d}\lambda \mathrm{d}\omega \, \mathrm{e}^{\mathrm{i}\lambda x + \mathrm{i}\omega y} \widehat{u}_2(t,\lambda,\omega)$$

$$= \frac{1}{2\pi} \int_{\mathbb{R}^2} \mathrm{d}\lambda \mathrm{d}\omega \int_0^t \mathrm{d}s \sum_{i=0}^{2} \mathrm{e}^{\mathrm{i}\lambda x + \mathrm{i}\omega y + (t-s)\phi_{0,0}(\lambda,\omega)} B_{2-i,i}(\mathrm{i}\partial_\lambda,\mathrm{i}\partial_\omega)\phi_{2-i,i}(\lambda,\omega)\widehat{u}_0(s,\lambda,\omega) \qquad \left.\vphantom{\int_0^t}\right\} =: u_2^A$$

$$+ \frac{1}{2\pi} \int_{\mathbb{R}^2} \mathrm{d}\lambda \mathrm{d}\omega \int_0^t \mathrm{d}s \sum_{i=0}^{1} \mathrm{e}^{\mathrm{i}\lambda x + \mathrm{i}\omega y + (t-s)\phi_{0,0}(\lambda,\omega)} B_{1-i,i}(\mathrm{i}\partial_\lambda,\mathrm{i}\partial_\omega)\phi_{1-i,i}(\lambda,\omega)\widehat{u}_1(s,\lambda,\omega) \qquad \left.\vphantom{\int_0^t}\right\} =: u_2^B$$

Comparing with the expression for u_1, we see that u_2^A is given by

$$u_2^A = \mathcal{L}_2^A(t,x,y,\mathcal{D}_x,\mathcal{D}_y) u_0(t,x,y),$$

$$\mathcal{L}_2^A(t,x,y,\lambda,\omega) := \int_0^t \mathrm{d}s \, \Phi_2(s,t,x,y,\lambda,\omega,-\mathrm{i}\partial_\lambda,-\mathrm{i}\partial_\omega).$$

For u_2^B, we compute

$$u_2^B = \frac{1}{2\pi} \int_{\mathbb{R}^2} \mathrm{d}\lambda \mathrm{d}\omega \int_0^t \mathrm{d}s \int_0^s \mathrm{d}r \sum_{i=0}^{1} \sum_{j=0}^{1} \mathrm{e}^{\mathrm{i}\lambda x + \mathrm{i}\omega y + (t-s)\phi_{0,0}(\lambda,\omega)} \cdots$$

$$B_{1-i,i}(\mathrm{i}\partial_\lambda,\mathrm{i}\partial_\omega)\phi_{1-i,i}(\lambda,\omega)\mathrm{e}^{(s-r)\phi_{0,0}(\lambda,\omega)} B_{1-j,j}(\mathrm{i}\partial_\lambda,\mathrm{i}\partial_\omega)\phi_{1-j,j}(\lambda,\omega)\widehat{u}_0(r,\lambda,\omega)$$

$$= \frac{1}{2\pi} \int_{\mathbb{R}^2} \mathrm{d}\lambda \mathrm{d}\omega \int_0^t \mathrm{d}s \int_0^s \mathrm{d}r \sum_{i=0}^{1} \sum_{j=0}^{1} \widehat{u}_0(r,\lambda,\omega)\phi_{1-j,j}(\lambda,\omega) \cdots$$

$$B_{1-j,j}(-\mathrm{i}\partial_\lambda,-\mathrm{i}\partial_\omega)\mathrm{e}^{(s-r)\phi_{0,0}(\lambda,\omega)}\phi_{1-i,i}(\lambda,\omega)B_{1-i,i}(-\mathrm{i}\partial_\lambda,-\mathrm{i}\partial_\omega)\mathrm{e}^{\mathrm{i}\lambda x + \mathrm{i}\omega y + (t-s)\phi_{0,0}(\lambda,\omega)}$$

$$= \frac{1}{2\pi} \int_{\mathbb{R}^2} \mathrm{d}\lambda \mathrm{d}\omega \, \mathrm{e}^{\mathrm{i}\lambda x + \mathrm{i}\omega y} \widehat{u}_0(t,\lambda,\omega) \int_0^t \mathrm{d}s \int_0^s \mathrm{d}r \cdots$$

$$\sum_{j=0}^{1} \phi_{1-j,j}(\lambda,\omega) \frac{B_{1-j,j}(-\mathrm{i}\partial_\lambda,-\mathrm{i}\partial_\omega)\mathrm{e}^{\mathrm{i}\lambda x + \mathrm{i}\omega y + (t-r)\phi_{0,0}(\lambda,\omega)}}{\mathrm{e}^{\mathrm{i}\lambda x + \mathrm{i}\omega y + (t-r)\phi_{0,0}(\lambda,\omega)}} \cdots$$

$$\sum_{i=0}^{1} \phi_{1-i,i}(\lambda,\omega) \frac{B_{1-i,i}(-\mathtt{i}\partial_\lambda, -\mathtt{i}\partial_\omega) \mathrm{e}^{\mathtt{i}\lambda x + \mathtt{i}\omega y + (t-s)\phi_{0,0}(\lambda,\omega)}}{\mathrm{e}^{\mathtt{i}\lambda x + \mathtt{i}\omega y + (t-s)\phi_{0,0}(\lambda,\omega)}} \cdots$$

$$= \frac{1}{2\pi} \int_{\mathbb{R}^2} \mathrm{d}\lambda \mathrm{d}\omega \, \mathrm{e}^{\mathtt{i}\lambda x + \mathtt{i}\omega y} \widehat{u}_0(t,\lambda,\omega) \cdots$$

$$\int_0^t \mathrm{d}s \int_0^s \mathrm{d}r \, \Phi_1(r,t,x,y,\lambda,\omega,-\mathtt{i}\partial_\lambda,-\mathtt{i}\partial_\omega) \Phi_1(s,t,x,y,\lambda,\omega,-\mathtt{i}\partial_\lambda,-\mathtt{i}\partial_\omega)$$

$$= \mathcal{L}_2^B(t,x,y,\mathcal{D}_x,\mathcal{D}_y) u_0(t,x,y),$$

where

$$\mathcal{L}_2^B(t,x,y,\lambda,\omega) := \int_0^t \mathrm{d}s \int_0^s \mathrm{d}r \, \Phi_1(r,t,x,y,\lambda,\omega,-\mathtt{i}\partial_\lambda,-\mathtt{i}\partial_\omega) \Phi_1(s,t,x,y,\lambda,\omega,-\mathtt{i}\partial_\lambda,-\mathtt{i}\partial_\omega).$$

Pulling both terms u_2^A and u_2^B together, we have

$$u_2(t,x,y) = u_2^A + u_2^B = \Big(\mathcal{L}_2^A(t,x,y,\mathcal{D}_x,\mathcal{D}_y) + \mathcal{L}_2^B(t,x,y,\mathcal{D}_x,\mathcal{D}_y) \Big) u_0(t,x,y)$$

$$= \mathcal{L}_2(t,x,y,\mathcal{D}_x,\mathcal{D}_y) u_0(t,x,y),$$

Next, we examine u_3. We have

$$u_3(t,x,y)$$

$$= \frac{1}{2\pi} \int_{\mathbb{R}^2} \mathrm{d}\lambda \mathrm{d}\omega \, \mathrm{e}^{\mathtt{i}\lambda x + \mathtt{i}\omega y} \widehat{u}_{3,0}(t,\lambda,\omega)$$

$$= \frac{1}{2\pi} \int_{\mathbb{R}^2} \mathrm{d}\lambda \mathrm{d}\omega \int_0^t \mathrm{d}s \sum_{i=0}^{3} \mathrm{e}^{\mathtt{i}\lambda x + \mathtt{i}\omega y + (t-s)\phi_{0,0}(\lambda,\omega)} B_{3-i,i}(\mathtt{i}\partial_\lambda, \mathtt{i}\partial_\omega) \phi_{3-i,i}(\lambda,\omega) \widehat{u}_0(s,\lambda,\omega) \qquad \Big\} =: u_3^A$$

$$+ \frac{1}{2\pi} \int_{\mathbb{R}^2} \mathrm{d}\lambda \mathrm{d}\omega \int_0^t \mathrm{d}s \sum_{i=0}^{2} \mathrm{e}^{\mathtt{i}\lambda x + \mathtt{i}\omega y + (t-s)\phi_{0,0}(\lambda,\omega)} B_{2-i,i}(\mathtt{i}\partial_\lambda, \mathtt{i}\partial_\omega) \phi_{2-i,i}(\lambda,\omega) \widehat{u}_1(s,\lambda,\omega) \qquad \Big\} =: u_3^B$$

$$+ \frac{1}{2\pi} \int_{\mathbb{R}^2} \mathrm{d}\lambda \mathrm{d}\omega \int_0^t \mathrm{d}s \sum_{i=0}^{1} \mathrm{e}^{\mathtt{i}\lambda x + \mathtt{i}\omega y + (t-s)\phi_{0,0}(\lambda,\omega)} B_{1-i,i}(\mathtt{i}\partial_\lambda, \mathtt{i}\partial_\omega) \phi_{1-i,i}(\lambda,\omega) \widehat{u}_2(s,\lambda,\omega) \qquad \Big\} =: u_3^C$$

Comparing with u_2^A and u_2^B we recognize

$$u_3^A = \mathcal{L}_{3,0}^A(t,x,y,\mathcal{D}_x,\mathcal{D}_y) u_0(t,x,y),$$

$$\mathcal{L}_3^A(t,x,y,\omega,\lambda) := \int_0^t \mathrm{d}s \, \Phi_3(s,t,x,y,\lambda,\omega,-\mathtt{i}\partial_\lambda,-\mathtt{i}\partial_\omega)$$

$$u_3^B = \mathcal{L}_3^B(t,x,y,\mathcal{D}_x,\mathcal{D}_y) u_0(t,x,y),$$

$$\mathcal{L}_{3,0}^B(t,x,y,\lambda,\omega) := \int_0^t \mathrm{d}s \int_0^s \mathrm{d}r \, \Phi_1(r,t,x,y,\lambda,\omega,-\mathtt{i}\partial_\lambda,-\mathtt{i}\partial_\omega) \Phi_2(s,t,x,y,\lambda,\omega,-\mathtt{i}\partial_\lambda,-\mathtt{i}\partial_\omega).$$

For u_3^C, we compute

$$u_3^C = \frac{1}{2\pi} \int_{\mathbb{R}^2} \mathrm{d}\lambda \mathrm{d}\omega \int_0^t \mathrm{d}s \int_0^s \mathrm{d}r \sum_{i=0}^{1} \sum_{j=0}^{2} \mathrm{e}^{\mathtt{i}\lambda x + \mathtt{i}\omega y + (t-s)\phi_{0,0}(\lambda,\omega)}$$

$$B_{1-i,i}(\mathtt{i}\partial_\lambda, \mathtt{i}\partial_\omega) \phi_{1-i,i}(\lambda,\omega) \mathrm{e}^{(s-r)\phi_{0,0}(\lambda,\omega)} B_{2-j,j}(\mathtt{i}\partial_\lambda, \mathtt{i}\partial_\omega) \phi_{2-j,j}(\lambda,\omega) \widehat{u}_0(s,\lambda,\omega)$$

$$+\frac{1}{2\pi}\int_{\mathbb{R}^2}\mathrm{d}\lambda\mathrm{d}\omega\int_0^t\mathrm{d}s\int_0^s\mathrm{d}r\int_0^r\mathrm{d}q\sum_{i=0}^1\sum_{j=0}^1\sum_{h=0}^1\mathrm{e}^{\mathrm{i}\lambda x+\mathrm{i}\omega y+(t-s)\phi_{0,0}(\lambda,\omega)}$$

$$B_{1-i,i}(\mathrm{i}\partial_\lambda,\mathrm{i}\partial_\omega)\phi_{1-i,i}(\lambda,\omega)\mathrm{e}^{(s-r)\phi_{0,0}(\lambda,\omega)}B_{1-j,j}(\mathrm{i}\partial_\lambda,\mathrm{i}\partial_\omega)\phi_{1-j,j}(\lambda,\omega)$$

$$\mathrm{e}^{(r-q)\phi_{0,0}(\lambda,\omega)}B_{1-h,h}(\mathrm{i}\partial_\lambda,\mathrm{i}\partial_\omega)\phi_{1-h,h}(\lambda,\omega)\widehat{u}_0(s,\lambda,\omega)$$

$$=\mathcal{L}_3^C(t,x,y,\mathcal{D}_x,\mathcal{D}_y)u_0,$$

where

$$\mathcal{L}_3^C(t,x,y,\lambda,\omega):=\int_0^t\mathrm{d}s\int_0^s\mathrm{d}r\,\Phi_2(r,t,x,y,\lambda,\omega,-\mathrm{i}\partial_\lambda,-\mathrm{i}\partial_\omega)\Phi_1(s,t,x,y,\lambda,\omega,-\mathrm{i}\partial_\lambda,-\mathrm{i}\partial_\omega)$$

$$+\int_0^t\mathrm{d}s\int_0^s\mathrm{d}r\int_0^r\mathrm{d}q\,\Phi_1(q,t,x,y,\lambda,\omega,-\mathrm{i}\partial_\lambda,-\mathrm{i}\partial_\omega)\Phi_1(r,t,x,y,\lambda,\omega,-\mathrm{i}\partial_\lambda,-\mathrm{i}\partial_\omega)$$

$$\Phi_1(s,t,x,y,\lambda,\omega,-\mathrm{i}\partial_\lambda,-\mathrm{i}\partial_\omega).$$

Pulling all three terms u_3^A, u_3^B and u_3^C together, we see that

$$u_3=u_3^A+u_3^B+u_3^C$$
$$=\Big(\mathcal{L}_3^A(t,x,y,\mathcal{D}_x,\mathcal{D}_y)+\mathcal{L}_3^B(t,x,y,\mathcal{D}_x,\mathcal{D}_y)+\mathcal{L}_3^C(t,x,y,\mathcal{D}_x,\mathcal{D}_y)\Big)u_0(t,x,y),$$
$$=\mathcal{L}_3(t,x,y,\mathcal{D}_x,\mathcal{D}_y)u_0(t,x,y),$$

Now, we compare (below, for simplicity, we remove the arguments x, y, λ, ω, $-\mathrm{i}\partial_\lambda$ and $-\mathrm{i}\partial_\omega$)

$$\mathcal{L}_1(t)=\int_0^t\mathrm{d}t_1\,\Phi_1(t_1,t),$$

$$\mathcal{L}_2(t)=\int_0^t\mathrm{d}t_1\,\Phi_2(t_1,t)+\int_0^t\mathrm{d}t_1\int_0^{t_1}\mathrm{d}t_2\,\Phi_1(t_2,t)\Phi_1(t_1,t),$$

$$\mathcal{L}_3(t)=\int_0^t\mathrm{d}t_1\,\Phi_3(t_1,t)+\int_0^t\mathrm{d}t_1\int_0^{t_1}\mathrm{d}t_2\,(\Phi_1(t_2,t)\Phi_1(t_1,t)+\Phi_1(t_2,t)\Phi_1(t_1,t))$$
$$+\int_0^t\mathrm{d}t_1\int_0^{t_1}\mathrm{d}t_2\int_0^{t_2}\mathrm{d}t_3\,\Phi_1(t_3,t)\Phi_1(t_2,t)\Phi_1(t_1,t).$$

From the above pattern, one guesses

$$\mathcal{L}_4(t)=\int_0^t\mathrm{d}t_1\,\Phi_4(t_1,t)+\int_0^t\mathrm{d}t_1\int_0^{t_1}\mathrm{d}t_2\,(\Phi_3(t_2,t)\Phi_1(t_1,t)+\Phi_1(t_2,t)\Phi_3(t_1,t)+\Phi_2(t_2,t)\Phi_2(t_1,t))$$
$$+\int_0^t\mathrm{d}t_1\int_0^{t_1}\mathrm{d}t_2\int_0^{t_2}\mathrm{d}t_3\,\big(\Phi_2(t_3,t)\Phi_1(t_2,t)\Phi_1(t_1,t)+\Phi_1(t_3,t)\Phi_2(t_2,t)\Phi_1(t_1,t)$$
$$+\Phi_1(t_3,t)\Phi_1(t_2,t)\Phi_2(t_1,t)\big)$$
$$+\int_0^t\mathrm{d}t_1\int_0^{t_1}\mathrm{d}t_2\int_0^{t_2}\mathrm{d}t_3\int_0^{t_3}\mathrm{d}t_4\,\Phi_1(t_4,t)\Phi_1(t_3,t)\Phi_1(t_3,t)\Phi_1(t_1,t).$$

And, indeed, one can easily check that this is correct. The general expression for $\mathcal{L}_n$ is that given in Theorem 9. Indeed, one can check that the expression given for u_n in Theorem 9 satisfies Cauchy problem (15).

C Implied volatility expressions

Assuming basis functions $B_{n,h}(x',y') = (x'-\bar{x})^n(y'-\bar{y})^h$ with $(\bar{x},\bar{y}) = (X_0,Y_0) := (x,y)$ we compute, explicitly

$$\sigma_0 = \sqrt{2a_{0,0}}, \qquad \sigma_1 = \sigma_{1,0} + \sigma_{0,1}, \qquad \sigma_2 = \sigma_{2,0} + \sigma_{1,1} + \sigma_{0,2},$$

where

$$\sigma_{1,0} = \left(\frac{a_{1,0}}{2\sigma_0}\right)(k-x), \qquad \sigma_{0,1} = \left(\frac{ta_{0,1}(c_{0,0}+2\alpha_{0,0})}{4\sigma_0}\right) + \left(\frac{a_{0,1}c_{0,0}}{2\sigma_0^3}\right)(k-x),$$

and

$$\sigma_{2,0} = \left(-\frac{t(12+t\sigma_0^2)a_{1,0}^2}{96\sigma_0} + \frac{1}{6}t\sigma_0 a_{2,0}\right) + \left(\frac{-3a_{1,0}^2 + 4\sigma_0^2 a_{2,0}}{12\sigma_0^3}\right)(k-x)^2$$

$$\sigma_{1,1} = \left(\frac{t\left(8\sigma_0^2 a_{1,1}c_{0,0} + a_{0,1}\left((4-t\sigma_0^2)a_{1,0}c_{0,0} - 8\sigma_0^2 c_{1,0}\right)\right)}{48\sigma_0^3}\right)$$

$$+ \left(\frac{t\left(4\sigma_0^2 a_{1,1}(c_{0,0}+2\alpha_{0,0}) + a_{0,1}\left(-5a_{1,0}(c_{0,0}+2\alpha_{0,0}) + 2\sigma_0^2(c_{1,0}+2\alpha_{1,0})\right)\right)}{24\sigma_0^3}\right)(k-x)$$

$$+ \left(\frac{2\sigma_0^2 a_{1,1}c_{0,0} + a_{0,1}\left(-5a_{1,0}c_{0,0} + \sigma_0^2 c_{1,0}\right)}{6\sigma_0^5}\right)(k-x)^2,$$

$$\sigma_{0,2} = \Bigg(-\frac{ta_{0,1}^2 b_{0,0}}{3\sigma_0^3} - \frac{t^2 a_{0,1}^2 b_{0,0}}{12\sigma_0} + \frac{ta_{0,2}b_{0,0}}{\sigma_0} + \frac{3ta_{0,1}^2 c_{0,0}^2}{8\sigma_0^5} - \frac{ta_{0,2}c_{0,0}^2}{3\sigma_0^3}$$

$$+ \frac{t^2 a_{0,2}c_{0,0}^2}{12\sigma_0} - \frac{ta_{0,1}c_{0,0}c_{0,1}}{6\sigma_0^3} + \frac{t^2 a_{0,1}c_{0,0}c_{0,1}}{24\sigma_0} - \frac{t^2 a_{0,1}^2 c_{0,0}\alpha_{0,0}}{8\sigma_0^3} + \frac{t^2 a_{0,2}c_{0,0}\alpha_{0,0}}{3\sigma_0}$$

$$+ \frac{t^2 a_{0,1}c_{0,1}\alpha_{0,0}}{12\sigma_0} - \frac{t^2 a_{0,1}^2 \alpha_{0,0}^2}{8\sigma_0^3} + \frac{t^2 a_{0,2}\alpha_{0,0}^2}{3\sigma_0} + \frac{t^2 a_{0,1}c_{0,0}\alpha_{0,1}}{12\sigma_0} + \frac{t^2 a_{0,1}\alpha_{0,0}\alpha_{0,1}}{6\sigma_0}\Bigg)$$

$$+ \Bigg(-\frac{3ta_{0,1}^2 c_{0,0}^2}{8\sigma_0^5} + \frac{ta_{0,2}c_{0,0}^2}{3\sigma_0^3} + \frac{ta_{0,1}c_{0,0}c_{0,1}}{6\sigma_0^3} - \frac{3ta_{0,1}^2 c_{0,0}\alpha_{0,0}}{4\sigma_0^5}$$

$$+ \frac{2ta_{0,2}c_{0,0}\alpha_{0,0}}{3\sigma_0^3} + \frac{ta_{0,1}c_{0,1}\alpha_{0,0}}{6\sigma_0^3} + \frac{ta_{0,1}c_{0,0}\alpha_{0,1}}{6\sigma_0^3}\Bigg)(k-x)$$

$$+ \left(\frac{-9a_{0,1}^2 c_{0,0}^2 + 2\sigma_0^2\left(2a_{0,1}^2 b_{0,0} + 2a_{0,2}c_{0,0}^2 + a_{0,1}c_{0,0}c_{0,1}\right)}{12\sigma_0^7}\right)(k-x)^2.$$

Higher order terms are too long to reasonably include in this text. However, σ_3 and (for local volatility models) σ_4 can be computed easily using the Mathematica code provided free of charge on the authors' websites.

http://explicitsolutions.wordpress.com
www.princeton.edu/~mlorig
www.math.unipd.it/~stefanop
www.dm.unibo.it/~pascucci

References

Alexander, C. and L. Nogueira (2004). Stochastic local volatility. *Proceedings of the Second IASTED Int. Conf. on Financial Engineering and Applications, Cambridge MA, USA*, 136–141.

Andersen, L. (2011). Option pricing with quadratic volatility: a revisit. *Finance and Stochastics 15*(2), 191–219.

Antonov, A. and M. Spector (2012, march). Advanced analytics for the sabr model. *SSRN*.

Baldeaux, J. and A. Badran (2012). Consistent modeling of vix and equity derivatives using a 3/2 plus jumps model. *arXiv preprint arXiv:1203.5903*.

Clark, I. (2010). *Foreign Exchange Option Pricing: A Practitioner's Guide*. Chichester: Wiley.

Corielli, F., P. Foschi, and A. Pascucci (2010). Parametrix approximation of diffusion transition densities. *SIAM J. Financial Math. 1*, 833–867.

Cox, J. (1975). Notes on option pricing I: Constant elasticity of diffusions. *Unpublished draft, Stanford University*. A revised version of the paper was published by the Journal of Portfolio Management in 1996.

Drimus, G. G. (2012). Options on realized variance by transform methods: a non-affine stochastic volatility model. *Quant. Finance 12*(11), 1679–1694.

Duffie, D., J. Pan, and K. Singleton (2000). Transform analysis and asset pricing for affine jump-diffusions. *Econometrica 68*(6), 1343–1376.

Estes, R. H. and E. R. Lancaster (1972). Some generalized power series inversions. *SIAM J. Numer. Anal. 9*, 241–247.

Ewald, C.-O. (2005). Local volatility in the Heston model: a Malliavin calculus approach. *J. Appl. Math. Stoch. Anal.* (3), 307–322.

Forde, M. and A. Jacquier (2009). Small-time asymptotics for implied volatility under the heston model. *International Journal of Theoretical and Applied Finance 12*(06), 861–876.

Forde, M. and A. Jacquier (2011). Small-time asymptotics for an uncorrelated local-stochastic volatility model. *Applied Mathematical Finance 18*(6), 517–535.

Forde, M., A. Jacquier, and R. Lee (2012). The small-time smile and term structure of implied volatility under the heston model. *SIAM Journal on Financial Mathematics 3*(1), 690–708.

Fouque, J.-P., M. Lorig, and R. Sircar (2012). Second order multiscale stochastic volatility asymptotics: Stochastic terminal layer analysis and calibration. *ArXiv preprint arXiv:1209.0697*.

Fouque, J.-P., G. Papanicolaou, R. Sircar, and K. Solna (2011). *Multiscale stochastic volatility for equity, interest rate, and credit derivatives*. Cambridge: Cambridge University Press.

Gao, K. and R. Lee (2011). Asymptotics of implied volatility to arbitrary order.

Gatheral, J., E. P. Hsu, P. Laurence, C. Ouyang, and T.-H. Wang (2012). Asymptotics of implied volatility in local volatility models. *Math. Finance 22*(4), 591–620.

Hagan, P., D. Kumar, A. Lesniewski, and D. Woodward (2002). Managing smile risk. *Wilmott Magazine 1000*, 84–108.

Hagan, P. and D. Woodward (1999). Equivalent black volatilities. *Applied Mathematical Finance 6*(3), 147–157.

Henry-Labordère, P. (2005). A general asymptotic implied volatility for stochastic volatility models. *eprint arXiv:cond-mat/0504317*.

Henry-Labordère, P. (2009). *Analysis, geometry, and modeling in finance: Advanced methods in option pricing*, Volume 13. Chapman & Hall.

Henry-Labordere, P. (2009). Calibration of local stochastic volatility models to market smiles: A Monte-Carlo approach. *RISK* (September), 112–117.

Heston, S. (1993). A closed-form solution for options with stochastic volatility with applications to bond and currency options. *Rev. Financ. Stud. 6*(2), 327–343.

Ikeda, N. and S. Watanabe (1989). *Stochastic differential equations and diffusion processes* (Second ed.), Volume 24 of *North-Holland Mathematical Library*. Amsterdam: North-Holland Publishing Co.

Jacquier, A. and M. Lorig (2013). The smile of certain lévy-type models. *ArXiv preprint arXiv:1207.1630*.

Johnson, W. P. (2002). The curious history of Faà di Bruno's formula. *Amer. Math. Monthly 109*(3), 217–234.

Lee, R. W. (2004). The moment formula for implied volatility at extreme strikes. *Mathematical Finance 14*(3), 469–480.

Lewis, A. (2007). Geometries and smile asymptotics for a class of stochastic volatility models.

Lipton, A. (2002). The vol smile problem. *Risk* (February), 61–65.

Lopez, J. L. and N. M. Temme (2002). Two-point Taylor expansions of analytic functions. *Studies in Applied Mathematics 109*(4), 297–311.

Lorig, M. (2012). Pricing derivatives on multiscale diffusions: An eigenfunction expansion approach. *to appear in Mathematical Finance*.

Lorig, M. (2013). The exact smile of certain local volatility models. *Quantitative Finance 13*(6), 897–905.

Lorig, M., S. Pagliarani, and A. Pascucci (2013). A family of density expansions for Lévy-type processes with default. *ArXiv preprint arXiv:1304.1849*.

Obloj, J. (2008, 5). Fine-tune your smile: Correction to Hagan et al. *Wilmott Magazine*.

Pagliarani, S. and A. Pascucci (2012). Analytical approximation of the transition density in a local volatility model. *Cent. Eur. J. Math. 10*(1), 250–270.

Pagliarani, S. and A. Pascucci (2013). Approximation formulas for local stochastic volatility with jumps. *SSRN preprint, available at `http://dx.doi.org/10.2139/ssrn.2077394`*.

Pagliarani, S., A. Pascucci, and C. Riga (2013). Adjoint expansions in local Lévy models. *SIAM J. Financial Math. 4*, 265–296.

Pascucci, A. (2011). *PDE and martingale methods in option pricing*, Volume 2 of *Bocconi & Springer Series*. Milan: Springer.

Riordan, J. (1946). Derivatives of composite functions. *Bull. Amer. Math. Soc. 52*, 664–667.
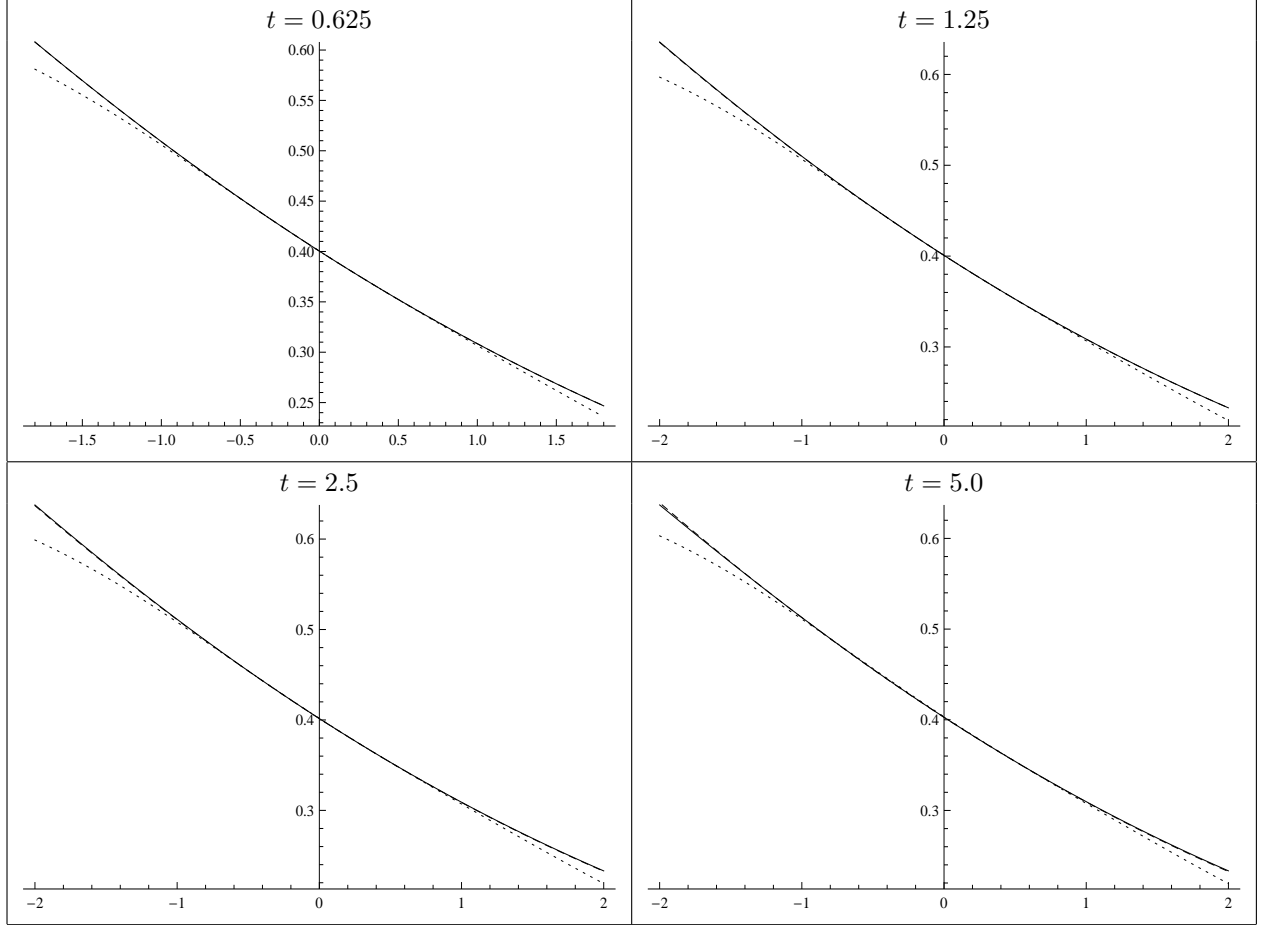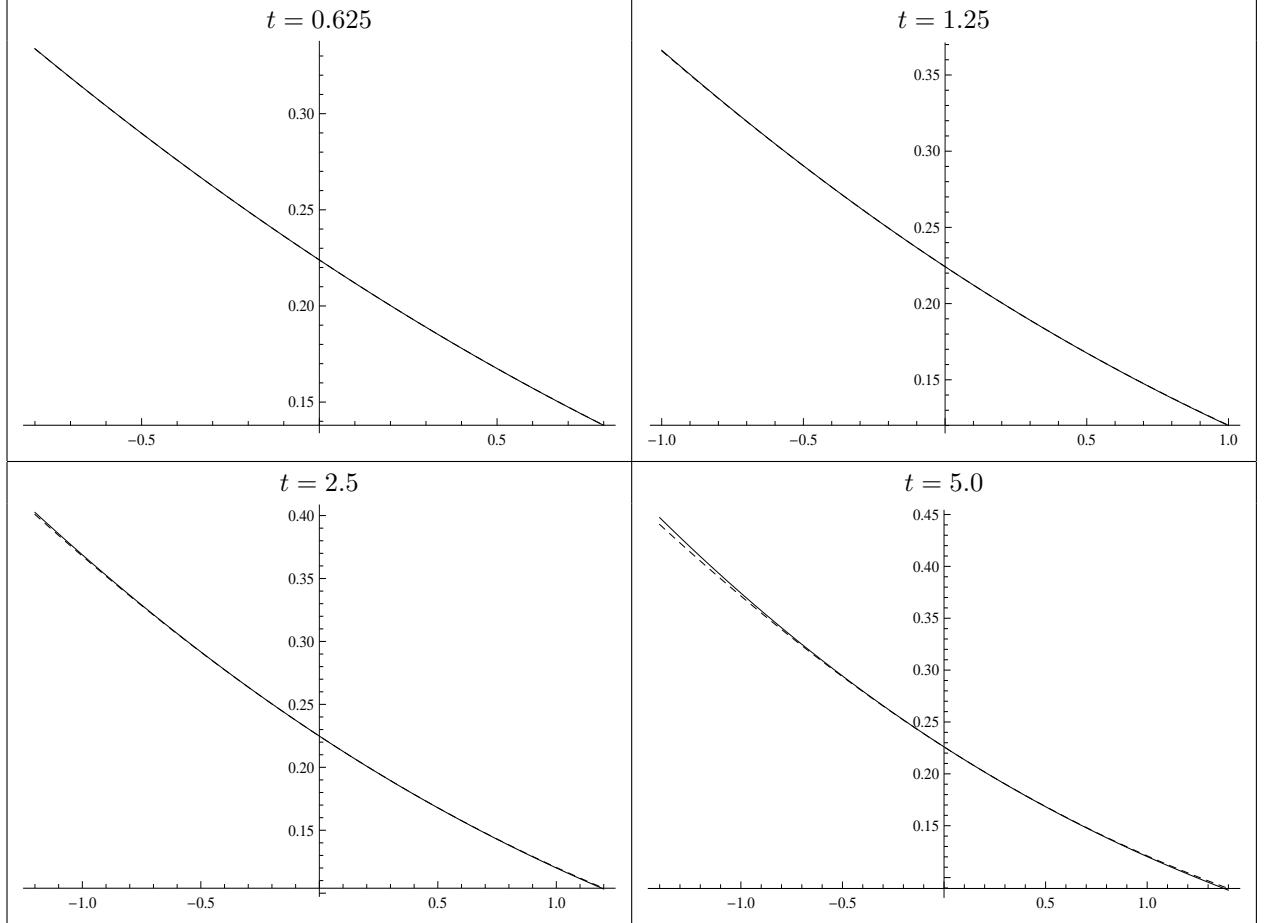
Figure 1: Implied volatility in the CEV model (44) is plotted as a function of log-moneyness $(k - x)$ for four different maturities t. The solid line corresponds to the exact implied volatility σ, which we obtain by computing the exact price u using (46) and then by solving (23) numerically. The dashed line (which is nearly indistinguishable from the solid line) corresponds to our third order implied volatility approximation $\sigma^{(3)}$, which we compute by summing the terms in (45). The dotted line corresponds to the implied volatility expansion σ^{HW} of Hagan and Woodward (1999), which is computed using (47). In all four plots we use the following parameters: $\beta = 0.5$, $\delta = 0.4$, $x = 0.0$. Relative errors for the two approximations $\sigma^{(3)}$ and σ^{HW} are given in Figure 2.
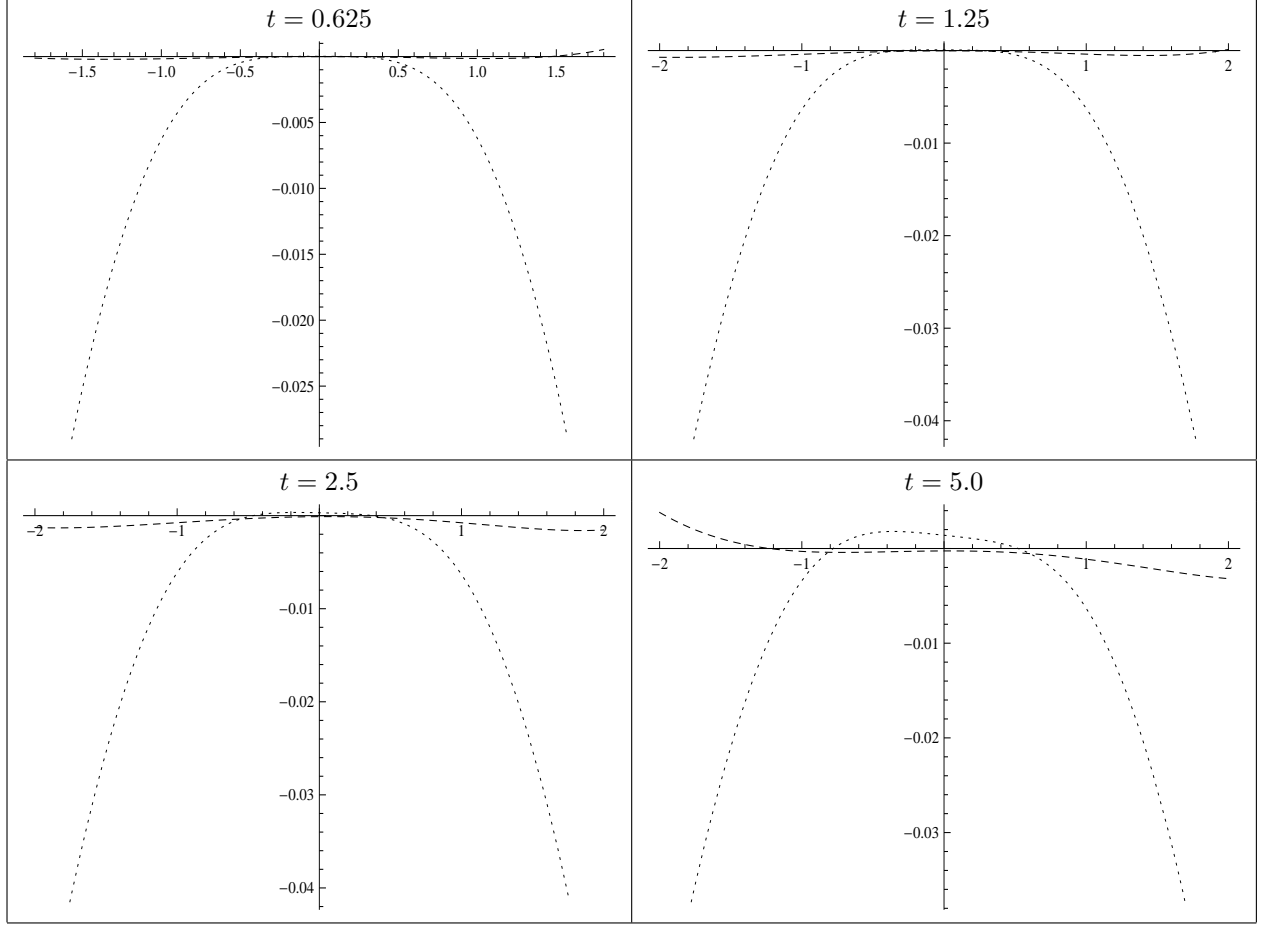
Figure 2: Relative error $(\sigma^{\text{Approx}} - \sigma)/\sigma$ is plotted as a function of log-moneyness $(k - x)$ for four different maturities t using two implied volatility approximations in the CEV model (44). The dashed line corresponds to the relative error of our third order implied volatility approximation: $\sigma^{\text{Approx}} = \sigma^{(3)}$. The dotted line corresponds to the relative error of the implied volatility approximation of Hagan and Woodward (1999): $\sigma^{\text{Approx}} = \sigma^{\text{HW}}$. The exact implied volatility σ is obtained by computing the exact price u using (46) and then by solving (23) numerically. Our third order implied volatility approximation $\sigma^{(3)}$ is computed by summing the terms in (45). The implied volatility expansion σ^{HW} of Hagan and Woodward (1999) is computed using (47). In all four plots we use the following parameters: $\beta = 0.5$, $\delta = 0.4$, $x = 0.0$. Observe that our third order implied volatility expansion $\sigma^{(3)}$ provides a better approximation of the true implied volatility σ than does the implied volatility expansion σ^{HW} of Hagan and Woodward (1999) for nearly all strikes and maturities.
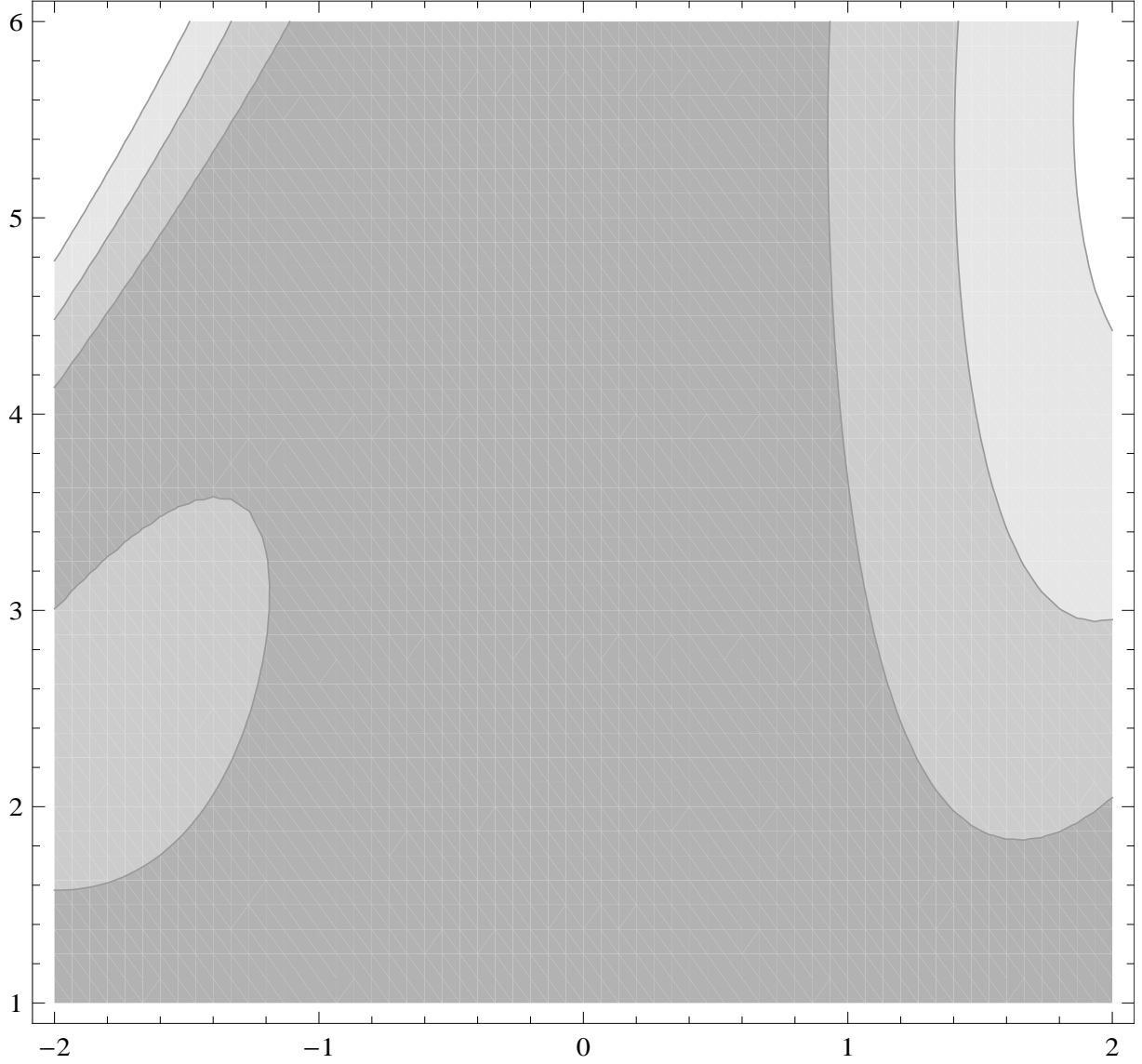
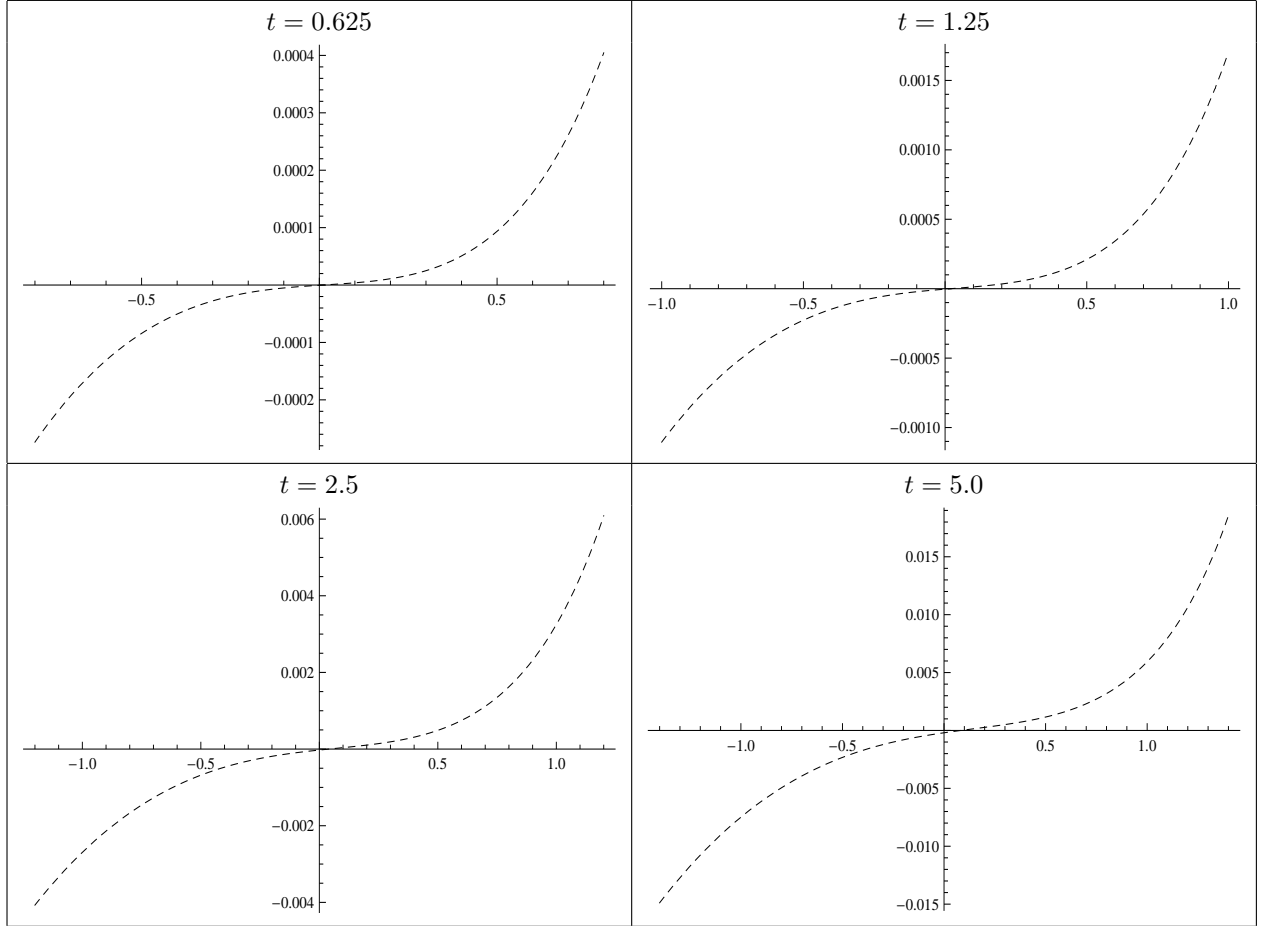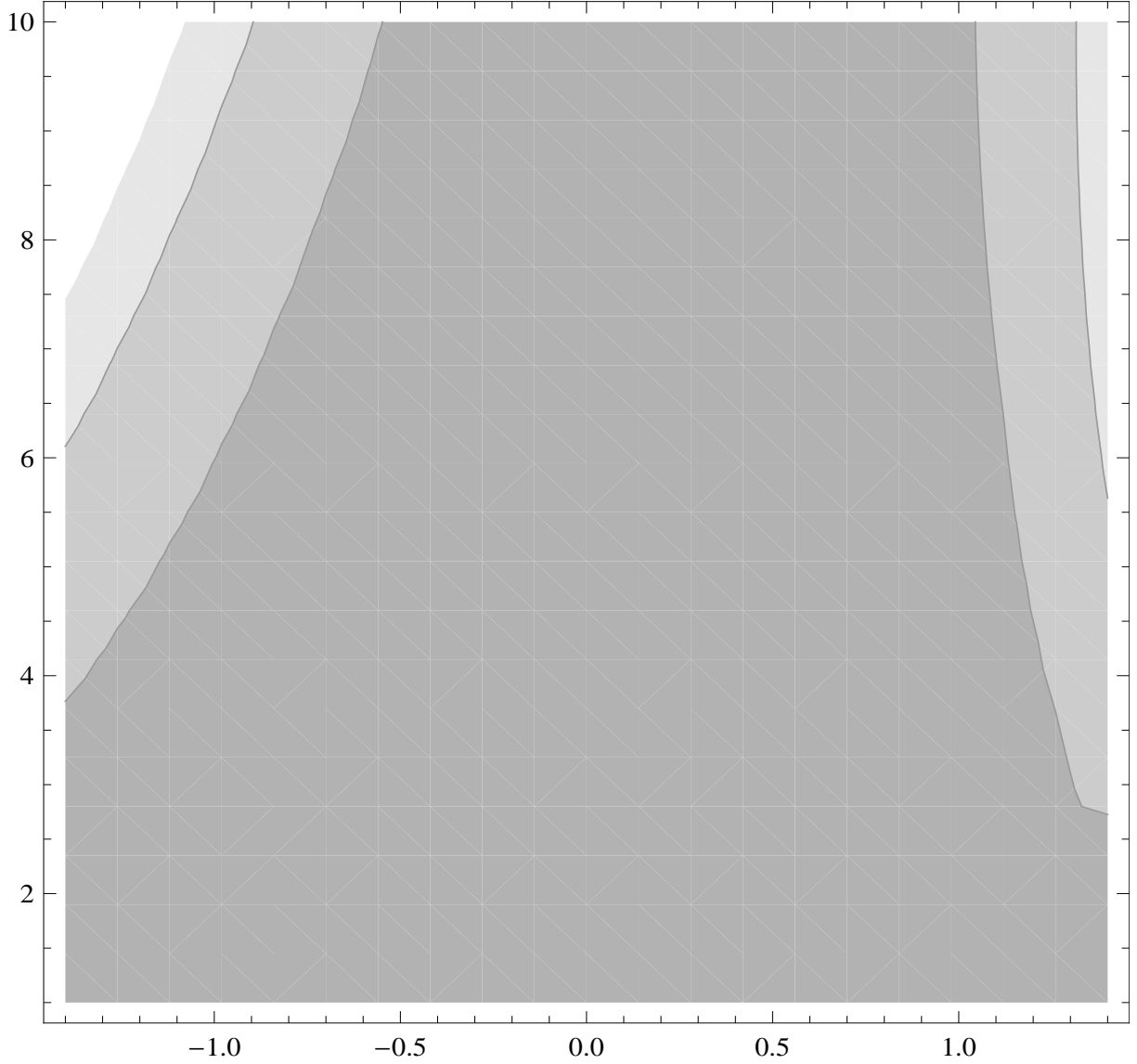Figure 3: For the CEV model (44), we plot the absolute value of the relative error $|\sigma^{(3)} - \sigma|/\sigma$ of our third order implied volatility approximation as a function of log-moneyness $(k-x)$ and maturity t. The horizontal axis represents log-moneyness $(k-x)$ and the vertical axis represents maturity t. Ranging from darkest to lightest, the regions above represent relative errors of $< 0.1\%$, 0.1% to 0.2%, 0.2% to 0.3% and $> 0.3\%$. The exact implied volatility σ is obtained by computing the exact price u using (46) and then by solving (23) numerically. Our third order implied volatility approximation $\sigma^{(3)}$ is computed by summing the terms in (45). We use the following parameters: $\beta = 0.5$, $\delta = 0.4$, $x = 0.0$.

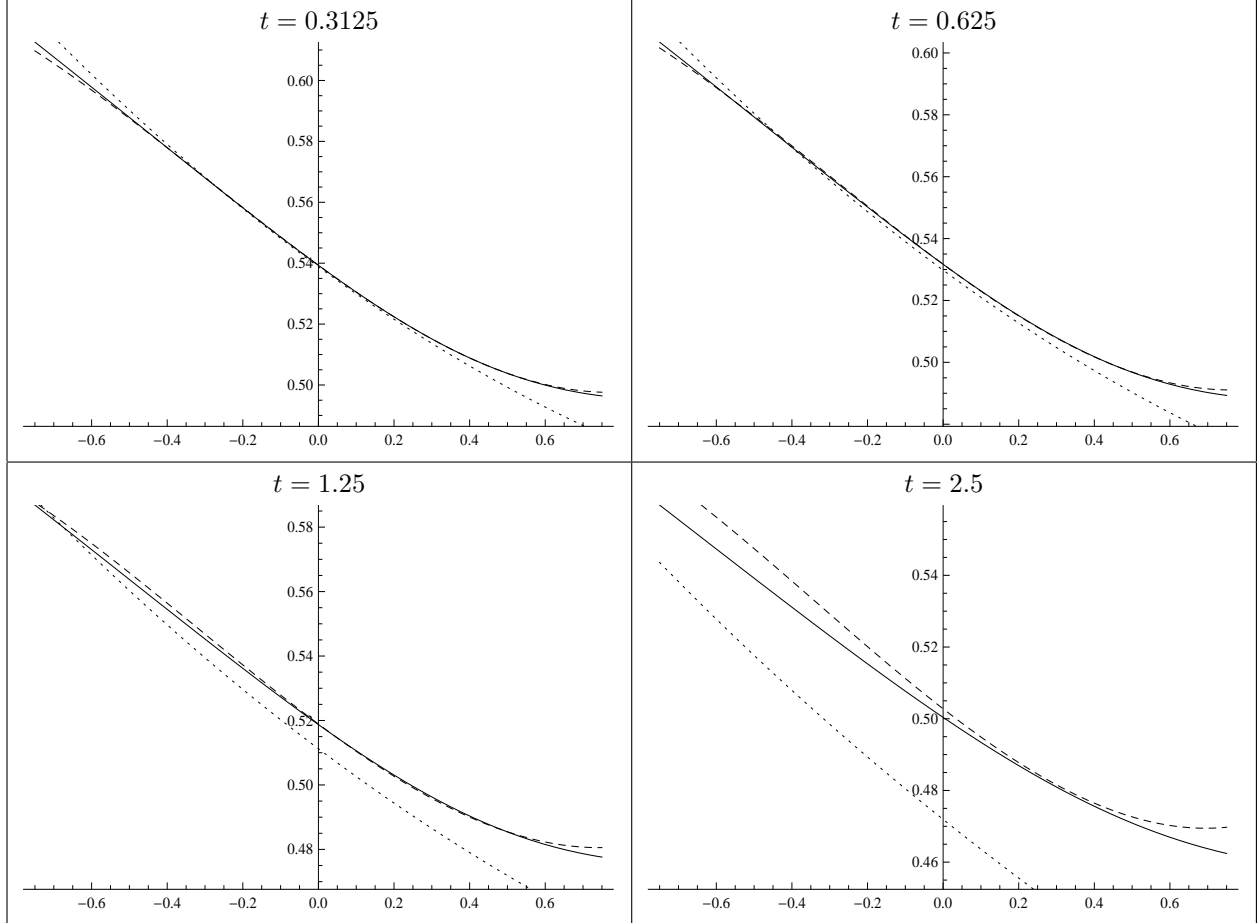Figure 4: Implied volatility in the Quadratic local volatility model (48) is plotted as a function of log-moneyness $(k - x)$ for four different maturities t. The solid line corresponds to the exact implied volatility σ, which we obtain by computing the exact price u using (50) and then by solving (23) numerically. The dashed line (which is nearly indistinguishable from the solid line) corresponds to our third order implied volatility approximation $\sigma^{(3)}$, which we compute by summing the terms in (49). In all four plots we use the following parameters: $L = 2.0$, $R = 15.0$, $\delta = 0.02$, $x = 0.0$. The relative error of the approximation $\sigma^{(3)}$ is given in Figure 5.

Figure 5: Relative error $(\sigma^{(3)} - \sigma)/\sigma$ of our third order implied volatility approximation is plotted as a function of log-moneyness $(k - x)$ for four different maturities t in the Quadratic local volatility model (48). The exact implied volatility σ is obtained by computing the exact price u using (50) and then by solving (23) numerically. Our third order implied volatility approximation $\sigma^{(3)}$ is computed by summing the terms in (49). In all four plots we use the following parameters: $L = 2.0$, $R = 15.0$, $\delta = 0.02$, $x = 0.0$.

Figure 6: For the Quadratic local volatility model (48) we plot the absolute value of the relative error $|\sigma^{(3)} - \sigma|/\sigma$ of our third order implied volatility approximation as a function of log-moneyness $(k - x)$ and maturity t. The horizontal axis represents log-moneyness $(k - x)$ and the vertical axis represents maturity t. Ranging from darkest to lightest, the regions above represent relative errors of $< 1\%$, 1% to 2%, 2% to 3% and $> 3\%$. The exact implied volatility σ is obtained by computing the exact price u using (50) and then by solving (23) numerically. Our third order implied volatility approximation $\sigma^{(3)}$ is computed by summing the terms in (49). We use the following parameters: $L = 2.0$, $R = 15.0$, $\delta = 0.02$, $x = 0.0$.

Figure 7: Implied volatility the Heston model (51) is plotted as a function of log-moneyness $(k - x)$ for four different maturities t. The solid line corresponds to the exact implied volatility σ, which we obtain by computing the exact price u using (53) and then by solving (23) numerically. The dashed line corresponds to our third order implied volatility approximation $\sigma^{(3)}$, which we compute by summing the terms in (52). The dotted line corresponds to the implied volatility expansion σ^{FJL} of Forde, Jacquier, and Lee (2012), which is computed using (54). In all four plots we use the following parameters: $\kappa = 0.33$, $\theta = 0.3$, $\delta = 0.44$, $\rho = -0.45$ $x = 0.0$, $y = \log \theta$. Note that our third order approximation of implied volatility $\sigma^{(3)}$ captures the at-the-money level and slope of the true implied volatility, as well as the smile effect, which is seen at large strikes. Relative errors for the two approximations $\sigma^{(3)}$ and σ^{FJL} are given in Figure 8.
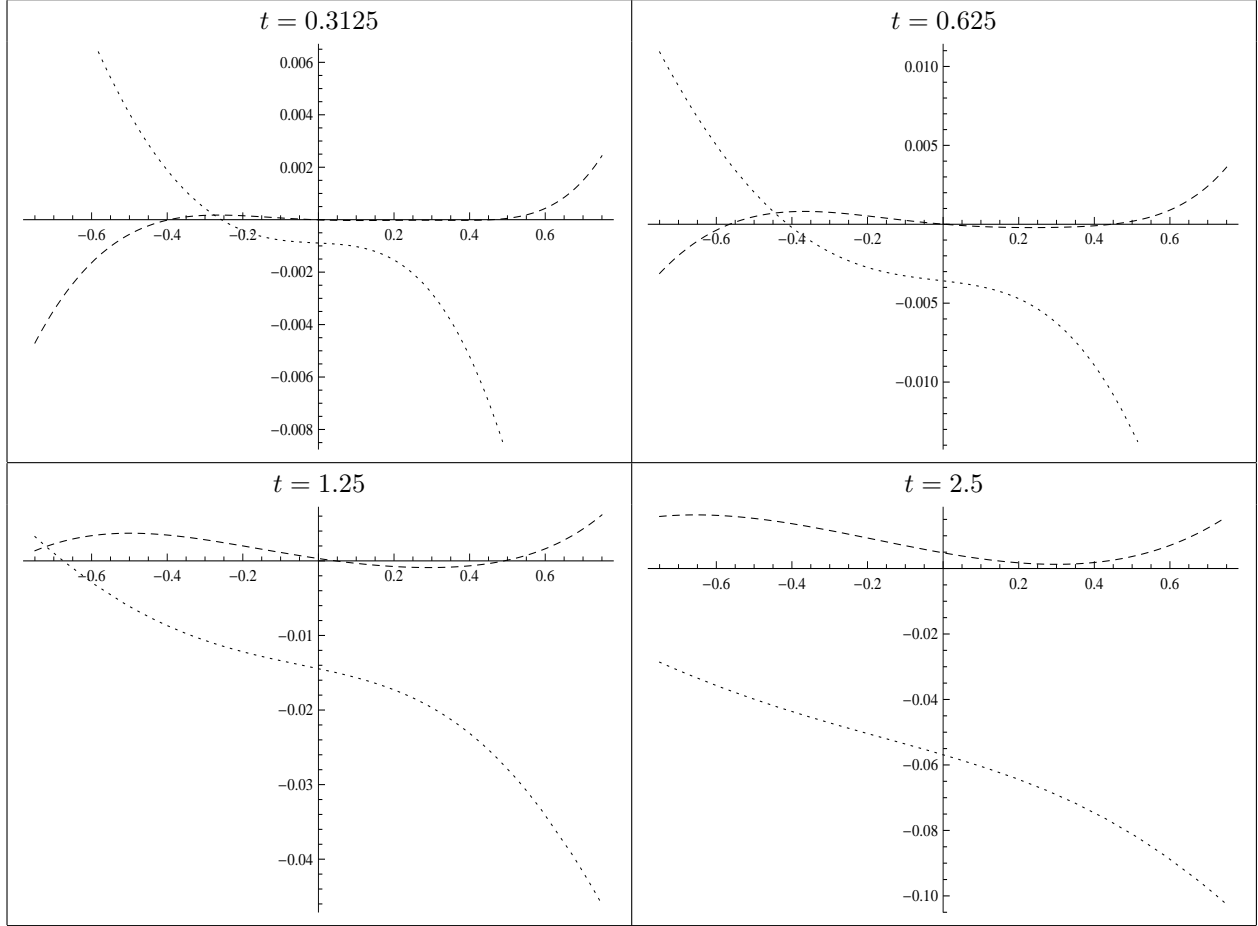
Figure 8: Relative error $(\sigma^{\mathrm{Approx}} - \sigma)/\sigma$ is plotted as a function of log-moneyness $(k - x)$ for four different maturities t using two implied volatility approximations in the Heston model (51). The dashed line corresponds to the relative error of our third order implied volatility approximation: $\sigma^{\mathrm{Approx}} = \sigma^{(3)}$. The dotted line corresponds to the relative error of the implied volatility approximation of Forde, Jacquier, and Lee (2012): $\sigma^{\mathrm{Approx}} = \sigma^{\mathrm{FJL}}$. The exact implied volatility σ is obtained by computing the exact price u using (53) and then by solving (23) numerically. Our third order implied volatility approximation $\sigma^{(3)}$ is computed by summing the terms in (52). The implied volatility expansion σ^{FJL} of Forde, Jacquier, and Lee (2012) is computed using (54). In all four plots we use the following parameters: $\kappa = 0.33$, $\theta = 0.3$, $\delta = 0.44$, $\rho = -0.45$ $x = 0.0$, $y = \log\theta$. Independent of the strike an maturity, the plots demonstrate that our third order implied volatility expansion $\sigma^{(3)}$ provides a better approximation to the true implied volatility σ than does the implied volatility expansion σ^{FJL} of Forde, Jacquier, and Lee (2012). This difference in quality between the two implied volatility expansions is most notable at higher strikes and longer maturities.
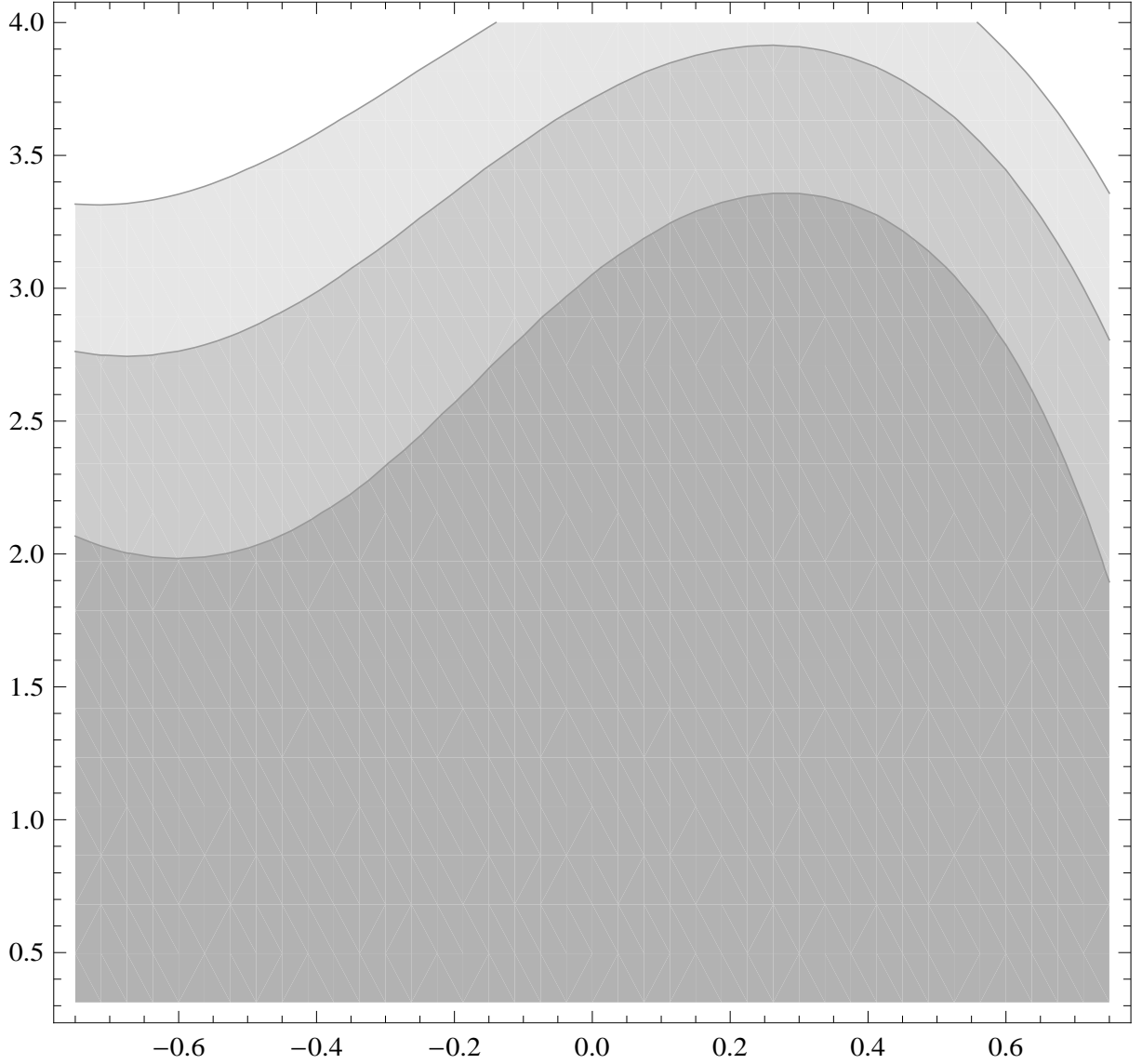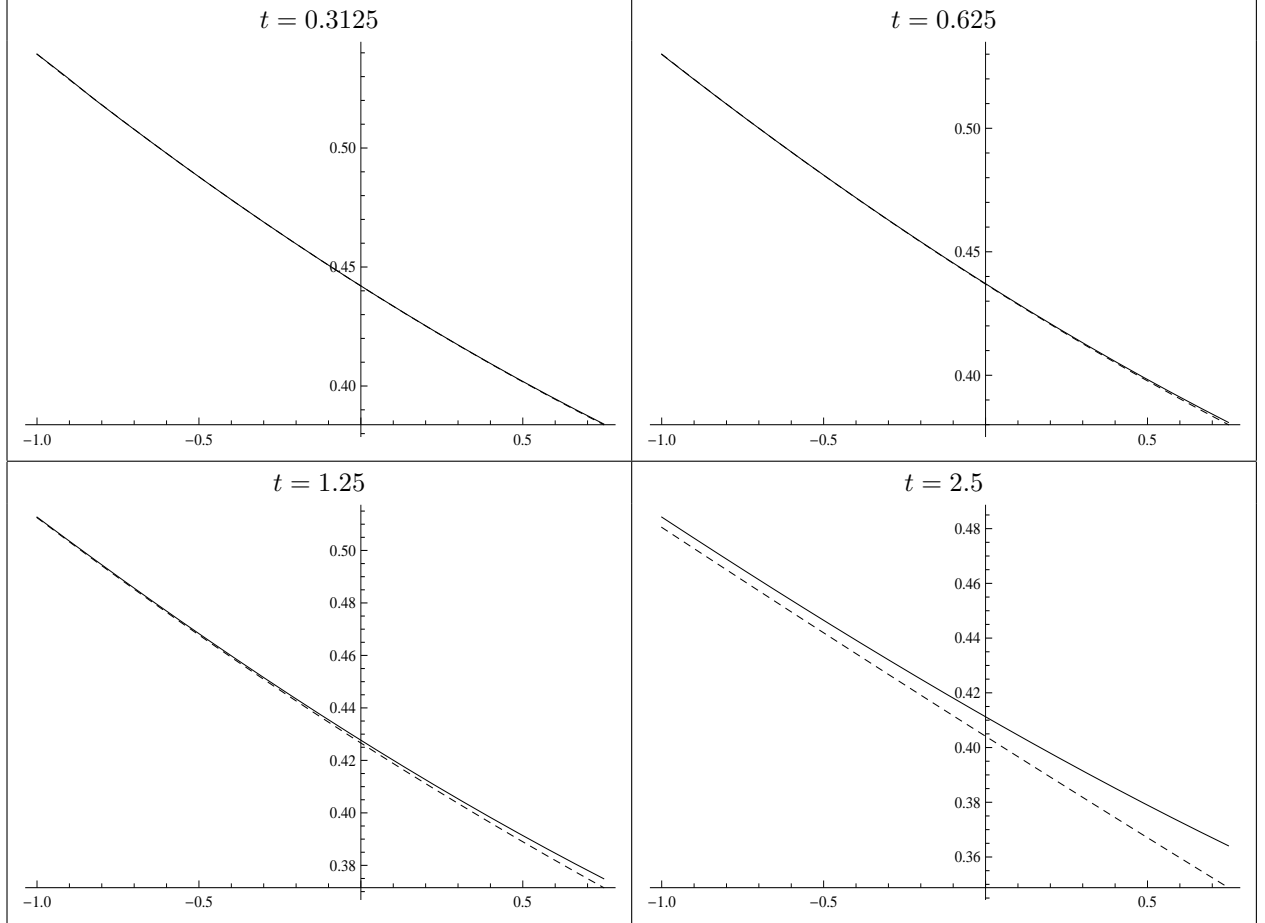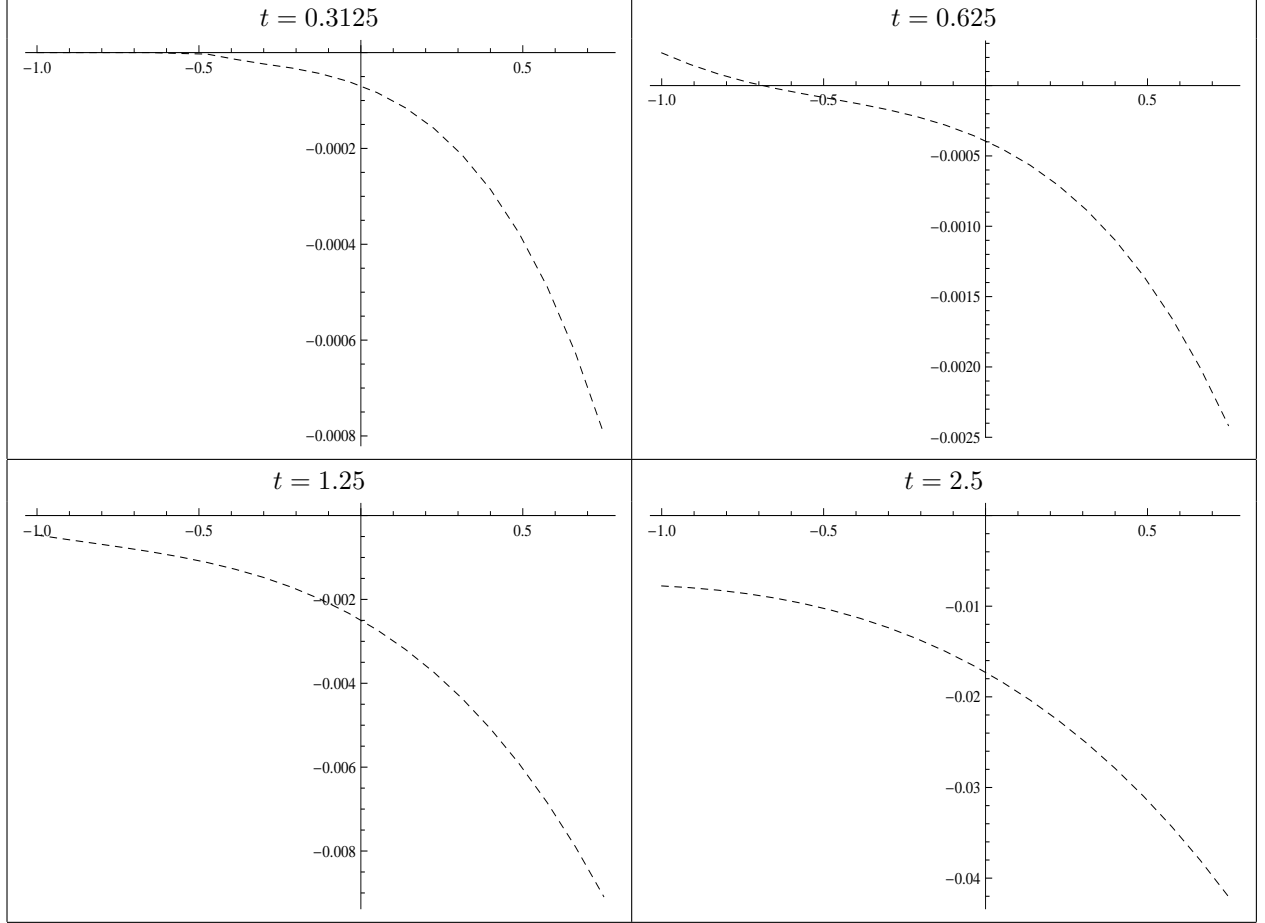
Figure 9: For the Heston model (51), we plot the absolute value of the relative error $|\sigma^{(3)} - \sigma|/\sigma$ of our third order implied volatility approximation as a function of log-moneyness $(k - x)$ and maturity t. The horizontal axis represents log-moneyness $(k - x)$ and the vertical axis represents maturity t. Ranging from darkest to lightest, the regions above represent relative errors of $< 1\%$, 1% to 2%, 2% to 3% and $> 3\%$. The exact implied volatility σ is obtained by computing the exact price u using (53) and then by solving (23) numerically. Our third order implied volatility approximation $\sigma^{(3)}$ is computed by summing the terms in (52). We use the following parameters: $\kappa = 0.33$, $\theta = 0.3$, $\delta = 0.44$, $\rho = -0.45$ $x = 0.0$, $y = \log \theta$.

Figure 10: Implied volatility in the 3/2 stochastic volatility model (55) is plotted as a function of log-moneyness $(k-x)$ for four different maturities t. The solid line corresponds to the exact implied volatility σ, which we obtain by computing the exact price u using (58) and then by solving (23) numerically. The dashed line corresponds to our third order implied volatility approximation $\sigma^{(3)}$, which we compute by summing the terms in (56). In all four plots we use the following parameters: $\kappa = 0.5$, $\theta = 0.2$, $\delta = 1.00$, $\rho = -0.8$ $x = 0.0$, $y = \log \theta$. Relative error for the approximation $\sigma^{(3)}$ is given in Figure 11.
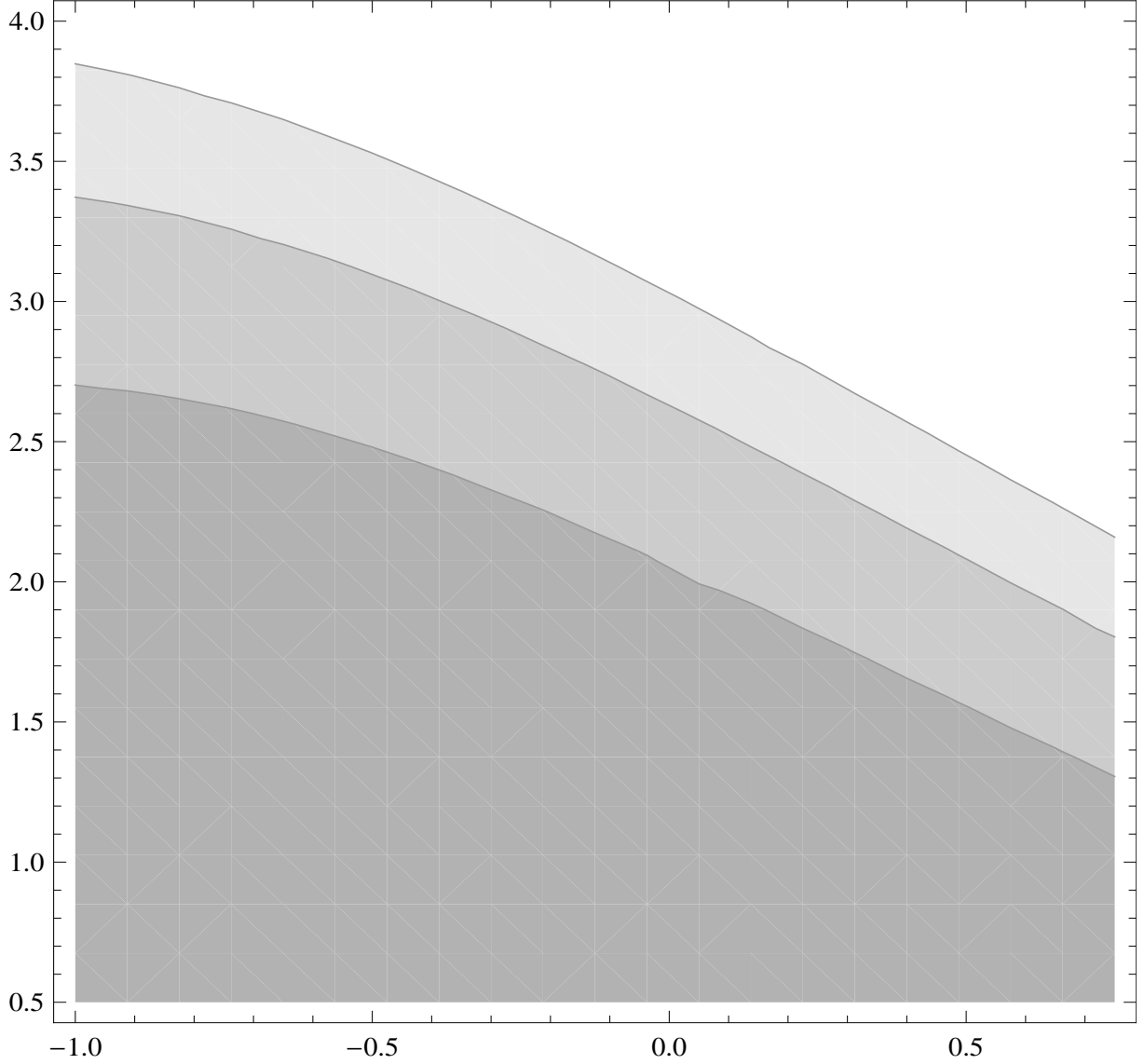
Figure 11: Relative error $(\sigma^{(3)} - \sigma)/\sigma$ of our third order implied volatility approximation is plotted as a function of log-moneyness $(k - x)$ for four different maturities t in the 3/2 stochastic volatility model (55). The exact implied volatility σ is obtained by computing the exact price u using (58) and then by solving (23) numerically. Our third order implied volatility approximation $\sigma^{(3)}$ is computed by summing the terms in (56). In all four plots we use the following parameters: $\kappa = 0.5$, $\theta = 0.2$, $\delta = 1.00$, $\rho = -0.8$ $x = 0.0$, $y = \log \theta$.

Figure 12: For the 3/2 stochastic volatility model (55), we plot the absolute value of the relative error $|\sigma^{(3)} - \sigma|/\sigma$ of our third order implied volatility approximation as a function of log-moneyness $(k - x)$ and maturity t. The horizontal axis represents log-moneyness $(k - x)$ and the vertical axis represents maturity t. Ranging from darkest to lightest, the regions above represent relative errors of $< 1\%$, 1% to 2%, 2% to 3% and $> 3\%$. The exact implied volatility σ is obtained by computing the exact price u using (53) and then by solving (23) numerically. Our third order implied volatility approximation $\sigma^{(3)}$ is computed by summing the terms in (52). We use the following parameters:$\kappa = 0.5$, $\theta = 0.2$, $\delta = 1.00$, $\rho = -0.8$ $x = 0.0$, $y = \log \theta$.

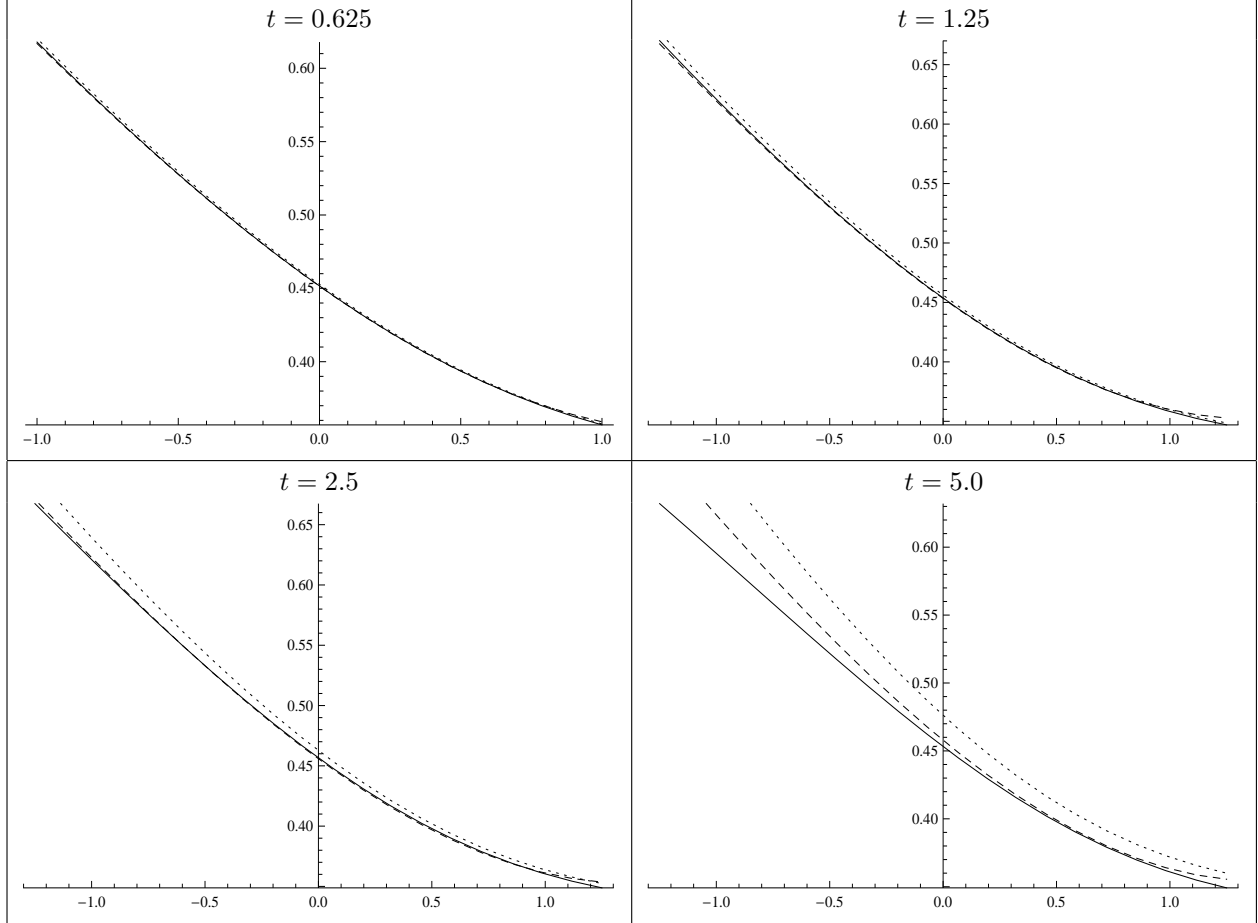Figure 13: Implied volatility the SABR model (59) is plotted as a function of log-moneyness $(k - x)$ for four different maturities t. The solid line corresponds to the exact implied volatility σ, which we obtain by computing the exact price u using (61) and then by solving (23) numerically. The dashed line corresponds to our third order implied volatility approximation $\sigma^{(3)}$, which we compute using (60). The dotted line corresponds to the implied volatility expansion σ^{HKLW} of Hagan, Kumar, Lesniewski, and Woodward (2002), which is computed using (62). In all four plots we use the following parameters: $\beta = 0.4$, $\delta = 0.25$, $\rho = 0.0$, $x = 0.0$, $y = -0.8$. For the two shortest maturities, both implied volatility expansions $\sigma^{(3)}$ and σ^{HKLW} provide an excellent approximation of the true implied volatility σ. However, for the two longest maturities, it is clear that our third order expansion $\sigma^{(3)}$ provides a better approximation to the true implied volatility σ than does the implied volatility expansion σ^{HKLW} of Hagan, Kumar, Lesniewski, and Woodward (2002). Relative errors for the two approximations $\sigma^{(3)}$ and σ^{HKLW} are given in Figure 14.
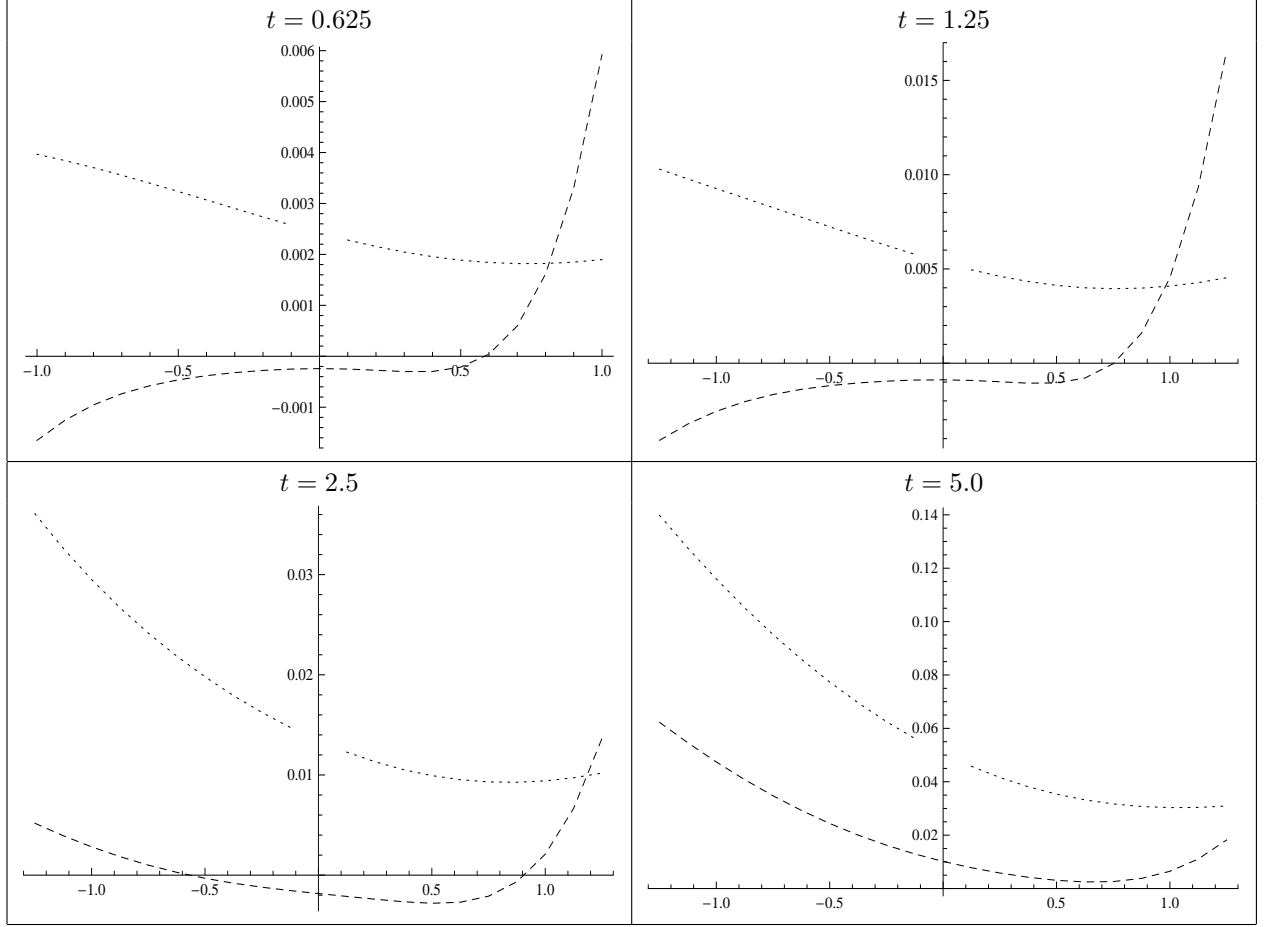
Figure 14: Relative error $(\sigma^{\mathrm{Approx}} - \sigma)/\sigma$ is plotted as a function of log-moneyness $(k-x)$ for four different maturities t using two implied volatility approximations in the SABR model (59). The dashed line corresponds to the relative error of our third order implied volatility approximation: $\sigma^{\mathrm{Approx}} = \sigma^{(3)}$. The dotted line corresponds to the relative error of the implied volatility approximation of Hagan, Kumar, Lesniewski, and Woodward (2002): $\sigma^{\mathrm{Approx}} = \sigma^{\mathrm{HKLW}}$. The exact implied volatility σ is obtained by computing the exact price u using (61) and then by solving (23) numerically. Our third order implied volatility approximation $\sigma^{(3)}$ is computed using (60). The implied volatility expansion σ^{HKLW} of Hagan, Kumar, Lesniewski, and Woodward (2002) is computed using (62). In all four plots we use the following parameters: $\beta = 0.4$, $\delta = 0.25$, $\rho = 0.0$, $x = 0.0$, $y = -0.8$. For the two shortest maturities, both implied volatility approximations $\sigma^{(3)}$ and σ^{HKLW} have a relative error of less than 1% for all $(k-x) \in (-1, 1)$. However, for $t = 2.5$, the relative error of $\sigma^{(3)}$ remains less than 1% for all $(k - x) \in (-1, 1)$ whereas the relative error of σ^{HKLW} ranges from 1% to 4%. The improvement marked by $\sigma^{(3)}$ is even more pronounced at $t = 5.0$.
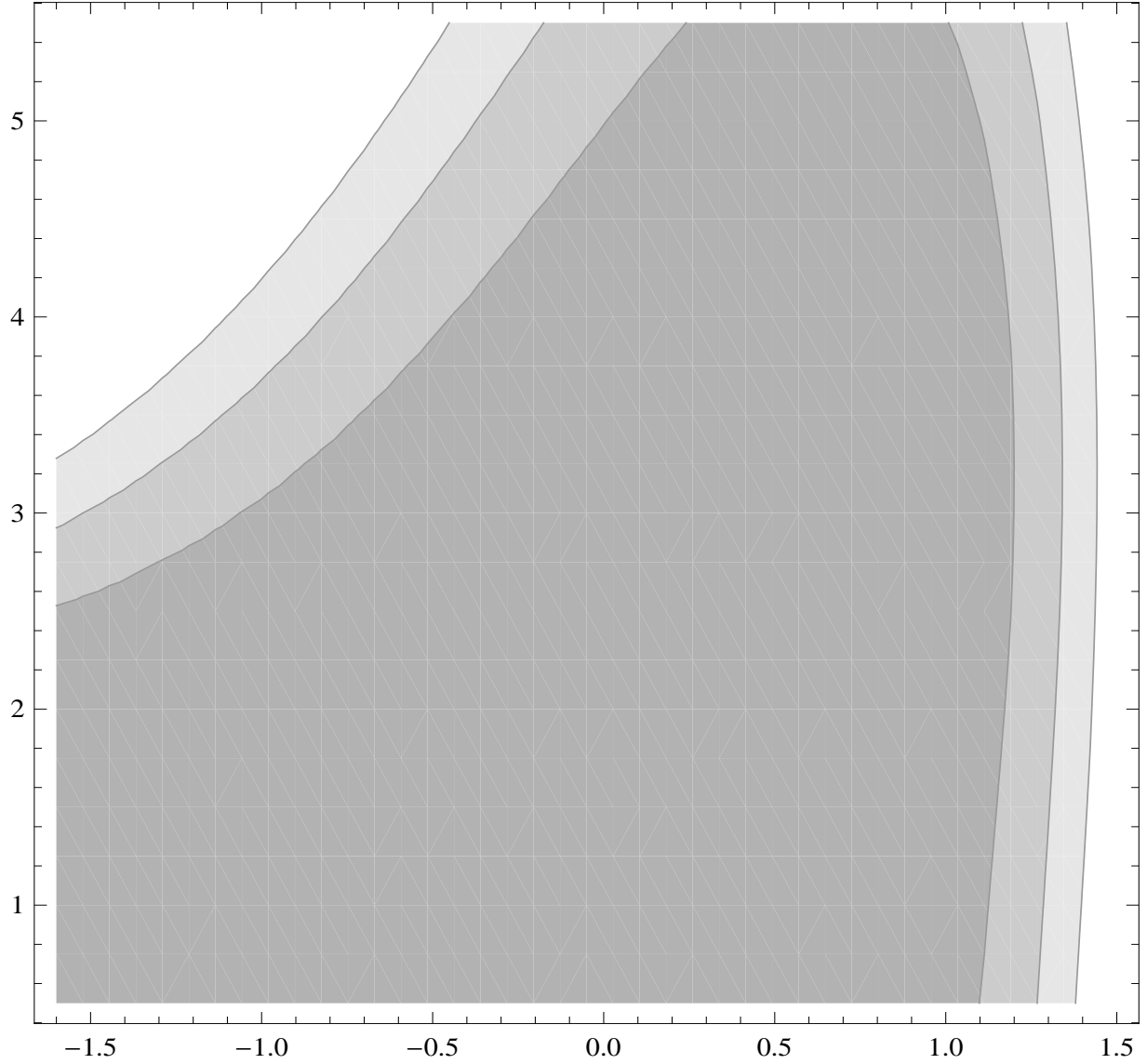
Figure 15: For the SABR model (59), we plot the absolute value of the relative error $|\sigma^{(3)} - \sigma|/\sigma$ of our third order implied volatility approximation as a function of log-moneyness $(k - x)$ and maturity t. The horizontal axis represents log-moneyness $(k - x)$ and the vertical axis represents maturity t. Ranging from darkest to lightest, the regions above represent relative errors of $< 1\%$, 1% to 2%, 2% to 3% and $> 3\%$. The exact implied volatility σ is obtained by computing the exact price u using (61) and then by solving (23) numerically. Our third order implied volatility approximation $\sigma^{(3)}$ is computed by summing the terms in (60). We use the following parameters: $\beta = 0.4$, $\delta = 0.25$, $\rho = 0.0$, $x = 0.0$, $y = -0.8$.